Applied Physics Reviews REVIEW scitation.org/journal/are

Stretchable sensors for environmental monitoring

Cite as: Appl. Phys. Rev. 6, 011309 (2019); doi: 10.1063/1.5085013
Submitted: 7 December 2018 · Accepted: 23 January 2019 ·
Published Online: 14 March 2019

Yang Yang[1] and Zhiqun Daniel Deng[1,2,a)]

AFFILIATIONS

[1]Energy and Environment Directorate, Pacific Northwest National Laboratory, Richland, Washington 99354, USA
[2]Department of Mechanical Engineering, Virginia Tech, Blacksburg, Virginia 24061, USA

[a)]Author to whom correspondence should be addressed: Zhiqun.deng@pnnl.gov

ABSTRACT

The development of flexible and stretchable sensors has been receiving increasing attention in recent years. In particular, stretchable, skin-like, wearable sensors are desirable for a variety of potential applications such as personalized health monitoring, human-machine interfaces, and environmental sensing. In this paper, we review recent advancements in the development of mechanically flexible and stretchable sensors and systems that can be used to quantitatively assess environmental parameters including light, temperature, humidity, gas, and pH. We discuss innovations in the device structure, material selection, and fabrication methods which explain the stretchability characteristics of these environmental sensors and provide a detailed and comparative study of their sensing mechanisms, sensor characteristics, mechanical performance, and limitations. Finally, we provide a summary of current challenges and an outlook on opportunities for possible future research directions for this emerging field.

TABLE OF CONTENTS

I. INTRODUCTION

The world's ecosystems regulate natural resources (soil, water, and air) upon which we all depend. These ecosystems also provide unique buffers against adverse effects such as extreme weather events, climatic changes, and ocean acidification.[1] Healthy ecosystems are essential for the well-being of human civilization and the long-term growth of economies. However, modern industrialization and urbanization have increasingly affected the integrity and functionality of vital natural assets and have also exacerbated environmental and human health risks and pollution.[2] Air pollution, lead poisoning, and hazardous waste cause fatal illnesses, create harmful living conditions, and may degrade or destroy ecosystems.[3–5] According to the World Bank, 60% to 70% of the world's ecosystems degrade faster than they can recover.[6] As stated in a report from the World Health Organization,[7] 12.6 million deaths were globally attributable to environmental factors in 2012, accounting for 23% of worldwide deaths and 26% of deaths among children under the age of five. Air pollution, contributing to 1 in 10 of all deaths worldwide, has become the fourth highest risk factor for premature deaths.[6] Overexposure of solar ultraviolet (UV) radiation causes acute and chronic health effects on the skin, eyes, and immune system.[8] The increasing contamination of freshwater and marine ecosystems with pollutants (industrial chemicals, consumer products, biocides, etc.) accelerates environmental changes throughout the world,[9,10] and the operation of hydroelectric dams blocks migration routes for fish and disrupts habitats,[11] threatening water and food security for human health and aquatic biodiversity.

Environmental monitoring using sensor technology is regarded as one of the key enablers for sustainably managing the environment and natural resources. This technology has been actively implemented for the last several decades by both the government and the industry.[12,13] However, because most of the devices currently used are bulky, fragile, and rigid, current monitoring methods, based upon sensors fabricated using semiconductor or printed circuit board (PCB) technology, are expensive, time intensive to use, limited in sampling and analytical techniques,[13] and incompatible for application with soft or complex-shaped objects.[14] Clearly, a demand exists for the development of next-generation environmental sensors that are not only fast, accurate, and versatile in terms of device performance but also lightweight, small, and soft in terms of their form factor. Such devices could be applied in curvilinear and complex shapes such as industrial infrastructures, robots, and natural assets and also could be worn on movable parts such as human or animal skin, organs, or textiles to allow *in situ* and real-time detection and diagnosis of environmental conditions and risks (Fig. 1).[12,13] The prospective use scenario of such devices should expand from the city, outskirt to the underwater environment toward the Internet of Things (IoT). For these advances to be realized, the major challenge to overcome is to move beyond electronics that are traditionally brittle and rigid to electronics that are flexible and stretchable.

During the last decade, substantial research and development efforts have focused on stretchable electronics.[18,19] This new class of electronics that are ultra-lightweight, possess low elastic modulus and high flexibility, and are stretchable has opened up new opportunities for novel sensor development for environmental monitoring. This emerging technology was invented to convert electronics that have traditionally been constrained to rigid and planar formats into the next generation which are bendable, compressible, stretchable, or formable into desired three-dimensional (3D) shapes and is leading a global revolution in electronic applications such as sensors and

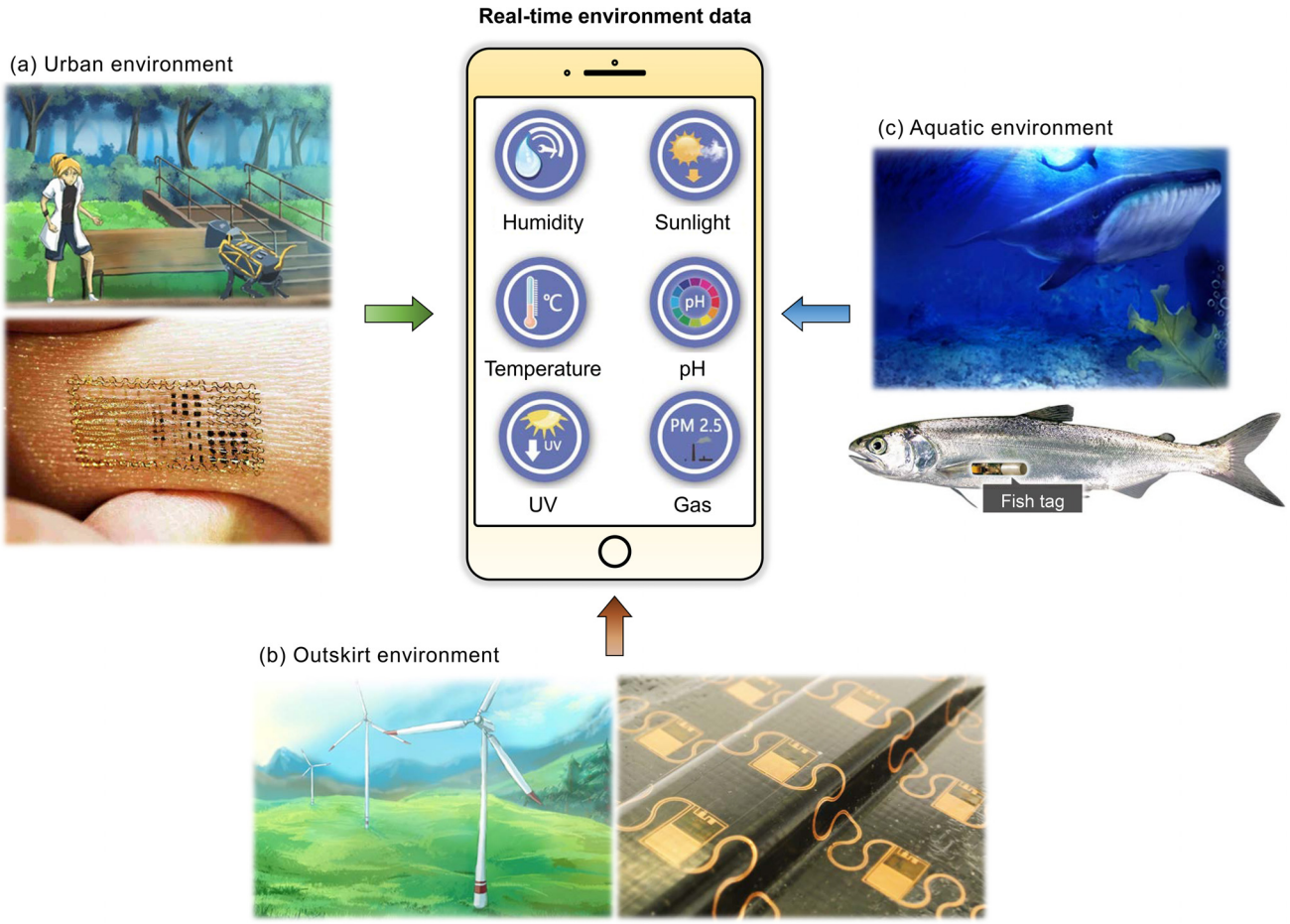

FIG. 1. Conceptual illustration of future sensor technology for monitoring environmental parameters such as humidity, temperature, UV, sunlight, pH, and gas enabled by wearable, integrable, stretchable sensors.[15–17] Prospective use scenarios are, but are not limited to, (a) attached on the human skin or robot body for urban environment monitoring, (b) integrated on man-made items or natural assets for outskirt environmental monitoring, and (c) embedded in aquatic animals for underwater environment monitoring. Reprinted with permission from D.-H. Kim *et al.*, Science **333**, 838 (2011). Copyright 2011 American Association for the Advancement of Science. Reprinted with permission from Y. Yang *et al.*, Adv. Electron. Mater. **4**(8), 1800071 (2018). Copyright 2018 John Wiley and Sons.

actuators,[19–25] energy harvesting and storage,[26–28] lighting,[29–31] and medical and healthcare.[32–36] Because they can be integrated with soft materials and curvilinear surfaces, stretchable electronics will provide the foundation for applications that exceed the scope of conventional semiconductors and PCB technologies. To accommodate mechanical deformation during stretching while maintaining the electrical performance and reliability of the system, either the materials or the structures need to be stretchable.[37] One approach is to engineer non-stretchable materials into novel structures and geometries, followed by encapsulation in an elastic material to achieve performance in a stretchable form.[38–40] An alternative route is to synthesize materials that are intrinsically stretchable at the macroscopic scale, including intrinsically stretchable materials such as hydrogels,[41–43] conducting and semiconducting polymers,[44,45] or nanocomposites composed of an elastomeric polymer matrix and randomly dispersed nanomaterials. In these nanocomposites, the network paths are rearranged when strain is applied to retain the electrical continuity. Nanomaterial dopants such as graphene, carbon nanotubes (CNTs),[46] and metallic and semiconducting nanowires (NWs)[47–50] could be used in these applications.

Although several reviews on the latest achievements in stretchable electronics have been reported, these reviews mainly focused on either stretchable electronics technology itself[51,52] or their applications for energy storage,[53] tactile sensors,[54] smart displays,[55] or health monitoring.[56,57] Conversely, a detailed overview of the development of stretchable sensors for monitoring environmental parameters has not yet been published. In this review, we discuss first-generation stretchable environmental sensors. We begin with a summary of the geometry designs and material innovations that enable these sensors. Then, we provide an overview of state-of-the-art stretchable devices and systems employed as light, temperature, humidity, pH, and gas sensors. The device structure, material selection, and fabrication methods that lead to stretchability for these sensors are discussed in each part, with a comparative discussion of their electrical and mechanical characteristics and performance. Our review concludes with an outlook on current challenges and opportunities for possible future research directions for this emerging field. Rather than showing all relevant previous results, this paper aims to present noteworthy work that may provide a glimpse of future trends of stretchable environmental sensors. We hope that our review will stimulate an exchange of ideas and generate greater interest in this emerging field.

II. STRUCTURES AND MATERIALS FOR STRETCHABLE ENVIRONMENTAL SENSORS

Two approaches have been developed for realizing first-generation stretchable environmental sensors.[37] The first approach, geometry engineering, involves modifying the structure and geometry of non-stretchable materials or systems, and so, they can be stretched without inducing significant local strain that would break the electrical conduction path. This type of stretchable electronics usually exhibits better electronic performance by taking advantage of conventional electronic materials. The second approach involves synthesizing materials that are intrinsically stretchable from a macroscopic viewpoint, thereby enabling intimate contact and integration to human skin or organs. Notwithstanding the higher stretchability and lower elastic modulus, devices obtained through this approach usually struggle to provide adequate electronic properties compared to the geometry-engineered counterparts. In this section, we summarize state-of-the-art advances in both strategies, especially those that have been explored to realize stretchable environmental sensors.

A. Geometry for stretchable environmental sensors

Geometry-engineered stretchable electronics (Fig. 2) achieve stretchability by optimizing the geometric structure of materials into buckled,[60] wavy,[58] crumpled,[64] in-plane meandered,[38] or island-bridge shapes.[38] The resulting structures can absorb the applied strain without inducing significant stress locally in the materials themselves. Historically, this strategy, along with novel fabrication and assembly schemes, was proposed to endow stretchability to conventional non-stretchable materials such as single-crystalline semiconducting nanomaterials, metallic films, or tracks.[38,58,60] Subsequently, the strategy has been extended to include intrinsically stretchable materials or nanocomposites that further enhance their mechanical compliance.

Figure 2(a) schematically illustrates the assembly process to build "wrinkled" stretchable electronics.[19] After the flexible thin-film transistor-integrated electronic foil is fabricated, it is laminated onto an elastomeric substrate pre-strained to a larger-than-normal length. After the pre-strain is released, the substrate returns to its original length and the ultrathin foil buckles into out-of-plane wrinkles that accommodate subsequent tensile strains to provide stretchability. When the wrinkled structure is stretched, it becomes flat. This approach leads to a structure [Fig. 2(b)] with high levels of mechanical durability that can withstand repeated compression and stretching to 100% tensile strain without compromising electronic performance. In addition to ultrathin plastic electronics, submicrometer single-crystal elements have been structured into shapes with microscale, periodic, wavy geometries supported by an elastomeric substrate using this approach [see the angled-view scanning electron microscopy (SEM) image in Fig. 2(c)].[58] This structure can be reversibly stretched and compressed to substantial strain levels without damaging the silicon. Later, Choi *et al.* introduced a biaxially stretchable form of single-crystalline silicon (Si) that consists of two-dimensionally buckled Si nanomembranes (Si NMs) on bidirectionally pre-strained polydimethylsiloxane (PDMS) [Fig. 2(d)].[59] In addition to being primarily used to achieve the stretchability in conventionally non-stretchable materials such as Si ribbons,[58] plastic electronics,[19] and Al_2O_3,[65] this approach has been adopted to enhance the mechanical performance of stretchable materials such as graphene,[66] NWs,[67] and conducting polymers.[68]

A controlled buckling strategy was proposed by Sun *et al.* in 2006 to obtain stretchable nanoribbons (NRs) of GaAs or Si with a "pop-up" configuration.[60] By combining a supportive pre-strained elastic substrate to induce local displacements and patterned surface chemistry to provide adhesion only at selected

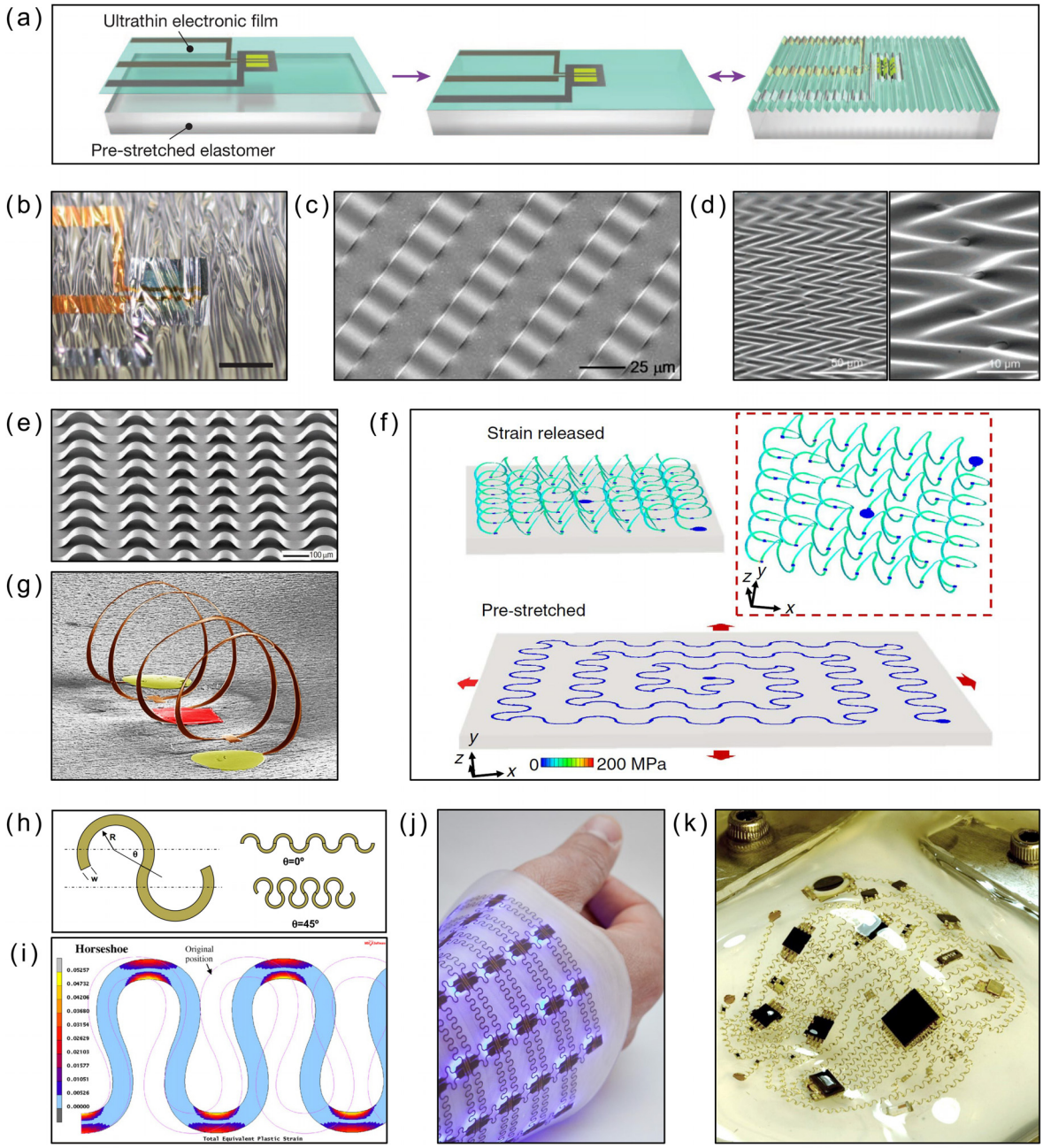

FIG. 2. Geometry engineering enables the development of stretchable environmental sensors. (a) Schematic of the process for building wrinkled stretchable electronics.[19] (b) Photograph of a wrinkled ultra-flexible transistor (scale bar: 1 mm).[19] Reprinted with permission from M. Kaltenbrunner *et al.*, Nature **499**, 458 (2013). Copyright 2013 Springer Nature. (c) Angled-view SEM image of wavy single-crystal Si ribbons.[58] Reprinted with permission from D. Y. Khang *et al.*, Science **311**, 208 (2006). Copyright 2006 American Association for the Advancement of Science. (d) Angled-view SEM images of 2D wavy Si NMs on PDMS.[59] Reprinted with permission from W. M. Choi *et al.*, Nano Lett. **7**, 1655 (2007). Copyright 2007 American Chemical Society. (e) Controlled buckling of Si ribbons on PDMS.[60] Reprinted with permission from Y. Sun *et al.*, Nat. Nanotechnol. **1**, 201 (2006). Copyright 2006 Springer Nature. (f) Process for assembly of 3D helical coils illustrated by finite element analysis. The color represents the magnitude of Mises stress in the metal layer.[61] (g) SEM image of a fabricated stretchable system with 3D conductive coils.[61] Reprinted with permission from K. I. Jang *et al.*, Nat. Commun. **8**, 15894 (2017). Copyright 2017 Author(s) licensed under a Creative Commons Attribution 4.0 International License. (h) Schematic of a horseshoe design.[62] (i) Plastic strain distribution in a horseshoe-shaped Cu conductor.[62] Reprinted with permission from M. Gonzalez *et al.*, Microelectron. Reliab. **48**, 825 (2008). Copyright 2008 Elsevier Ltd. (j) The concept of island-bridge design is demonstrated by a stretchable blue-light therapy device developed by imec.[63] Reprinted with permission from J. van den Brand *et al.*, Solid State Electron. **113**, 116 (2015). Copyright 2015 Elsevier Ltd. (k) Island-bridge configured freely deformed 3D coil-based circuit.[61]

areas, this approach allows the active circuitry to delaminate from the elastic substrate partially. For example, the Si ribbon structure on a PDMS with 50% tensile pre-strain [Fig. 2(e)] can be stretched up to 100%, compressed up to 25%, and bent with the curvature radius down to 5 mm. In 2015, Xu *et al.* further expanded the original design concept and the assembly process to achieve two-dimensional (2D) to 3D transformations for complex-shaped structures.[69] The design concept and assembly process are illustrated by the finite element simulation [Fig. 2(f)]. Rather than using a straight-line interconnect with a pre-strained substrate, a 2D filamentary serpentine precursor was patterned and bonded to an underlying biaxially pre-strained elastomeric substrate at selected locations. After the pre-strain was released, the 2D film popped up into a 3D configuration and formed 3D helical coils [Fig. 2(g)] by relaxation of the substrate to its initial, unstretched state.[61]

In-plane stretchable topologies, including serpentine, meander, and horseshoe, constitute another primary strategy for achieving geometry-engineered stretchable electronics.[38] Unlike a conventional electronic circuit, the signal carrying lines between two points is a periodic undulating metal track rather than a straight line. In this way, a configuration resembling a 2D spring is obtained. This design permits much higher deformations compared to a straight line. Common metal conductors (Ag, Cu, Ni, and Pt) have minimal elastic ranges. Therefore, the design of an appropriate shape is essential to achieve stretchability for the conductors. Several researchers have studied the optimizations of in-plane shapes to reduce local stress concentrations.[62,70–74] Gonzalez *et al.* numerically studied the plastic strain distribution in a copper (Cu) conductor line for three distinct conductor shapes: (1) elliptical, (2) serpentine, and (3) horseshoe [Fig. 2(h)].[62] The critical design parameters for a horseshoe shape are its inner radius (R), joining angle (θ), and width of the metal track (w). According to the finite element analysis [Fig. 2(i)], a horseshoe is the optimal shape of the three candidates as the stress is distributed in an extended part of the conductor.[62] In 2011, Hsu *et al.* improved the performance of the in-plane stretchable interconnect by using polyimide (PI) as the substrate beneath the conductor material.[71] Statistical analysis showed that the PI width played the most significant role among the different design parameters. By increasing the PI width, the stretchability and the fatigue lifetime of the system are increased because of the reduced plastic strain in the conductor stripes. When responding to the applied strain, these geometries not only elongate in-plane but also buckle out-of-plane. Hsu *et al.* further studied the influence of encapsulation on deformation behavior and failure mechanisms of stretchable interconnects.[72] Their numerical and experimental results revealed that the out-of-plane deformation and in-plane geometrical opening are reduced by adding a top encapsulation layer on the stretchable interconnect. Further enhanced stretchability could be achieved when these horseshoe or serpentine microstructures are bonded to pre-strained elastomers.[74] In 2014, Fan *et al.* proposed self-similar fractal design concepts for stretchable electronics.[73] In particular, he demonstrated the utility of several fractal constructs along with a wide range of topologies to yield space-filling geometries for 2D deterministic systems. Compared to previous periodic horseshoe or serpentine shapes, fractal designs can be engineered to accommodate enhanced elastic strain along a selected dimension and support biaxial, radial, and other deformation modes.

Geometry-engineering-based stretchability comes with a set of requirements. (1) Processing steps such as film deposition and patterning techniques should be developed for each new material; (2) the processing steps should be compatible with complex, multilayered, high-performance integrated circuits; and (3) there should be a large enough area to be allocated to the stretchable interconnects that are space-demanding. Simultaneously fulfilling all these requirements is economically and technologically challenging. To bypass these challenges, the island-bridge concept has been extensively adopted by the research community.[75] The principle behind this concept is demonstrated through the example of a large-area array of stretchable light-emitting diodes.[63] This array [Fig. 2(j)] is divided into functional islands containing the off-the-shelf rigid and non-stretchable light-emitting diodes and stretchable interconnects with a horseshoe or serpentine shape. Upon stretching the circuit, the stretchable interconnects deform effectively both in-plane and out-of-plane and isolate the functional islands from the applied strain, thereby achieving stretchability from a system standpoint. One-time elongations of up to 60% have been demonstrated using this approach when encapsulated in an elastomer (e.g., PDMS) and ~100% when freestanding structures are considered.[76] Major advantages of this approach include (1) use of commercially available, off-the-shelf electronics, such as passive components, memories, and lighting, computation, and communication chips [Fig. 2(k)],[61] (2) better space economy because fewer stretchable interconnections are required in the system, and (3) compatibility with both geometry-engineered and material-inspired stretchable materials. Among the technologies employing island-bridge configurations, PCB technology inspired stretchable circuits have attracted considerable attention as they are scalable to an industrial scale manufacturing environment,[77,78] allowing standard PCB processes for off-the-shelf component integration, permitting precision alignment steps, and covering a wide range of encapsulation material choices, such as PDMS, polyurethane (PU), polystyrene, and thermoplastic composites. In light of this technology, various stretchable devices have been realized including light sensors,[79] temperature sensors,[80] humidity sensors,[81] pH sensors,[82] and gas sensors.[83]

Moreover, by employing the island-bridge configuration, 3D circuits with integrated sensors and integrated circuits, either in a permanent curvilinear or in a soft and stretchable form, have been demonstrated. These devices achieved their stretchability from in-plane geometry,[17,84–87] out-of-plane geometry,[79] or a combination of the two geometries.[61] Yang *et al.* and Plovie *et al.* documented an easily scalable approach that involves the combined use of the PCB technology inspired stretchable circuit and thermoforming technology for the creation of 3D sensory polymers and composites.[17,84–86] This technology begins with fabricating the circuit on a rigid and planar carrier board, then transferring the circuit, and sandwiching it between thermoplastic polymers or composites using a

lamination process. The final thermoforming step shapes the sandwich structure by heating the encapsulating polymer beyond its glass transition temperature and pushing the polymer layers and the circuit toward the mold. Biswas *et al.* also produced metamorphic electronics that can take on 3D shapes.[87]

B. Materials for stretchable environmental sensors

The materials that enable stretchable environmental sensors can be divided into two groups: (1) materials with intrinsic stretchability and (2) stretchable nanocomposites assembled from the elastomeric polymer matrix and fillers, ranging from zero-dimensional, one-dimensional (1D) to 2D nanomaterials depending on their physical shapes. The properties (electronic, chemical, thermal, mechanical, optical, etc.) of these novel materials and their fabrication and assembly processes play an essential role in the design and performance of stretchable environmental sensors.

Because they can withstand large deformations while retaining electrical continuity, liquid metals are compelling materials for the manufacture of stretchable environmental sensors.[88] Liquid metals, such as eutectic alloys of gallium and indium (EGaIN),[89] provide the best combination of conductivity and stretchability because the liquid is inherently more deformable than solid metals. When liquid metals are embedded in microfluidic channels [Fig. 3(a)] made of elastomers such as Ecoflex and PDMS,[90] a conductive channel that can withstand several hundred percent stretchability could be realized because of the ability of the liquid metal to reconfigure its shape. Several methods have been employed to pattern the gallium liquid metal, including lithography-enabled, injection, additive approaches that deposit the material only in desired places and subtractive approaches that selectively remove the material.[88] Temperature, humidity, and gas sensors are examples of liquid metal applications.[91,92] Ota *et al.* developed a stretchable sensor platform that integrates liquid metal electrodes and various ionic liquids. By measuring changes in capacitance and conductance of the ionic liquid, the sensor can selectively measure different stimuli, including temperature, humidity, and the oxygen content.[92] Nonetheless, for a long-term use of liquid metals for environmental sensing, challenges associated with the integrity of liquid metal within the encapsulation must be overcome, and so, the liquid metal structure does not leak either internally or externally.[88] Also, the potential toxicity of gallium to humans has been identified as a concern regarding wearable electronics.[88]

Innovative nanomaterials represent another promising direction that could lead to stretchable environmental sensors. Over the last decade, significant advances have been made in our understanding of nanoscale phenomena, innovative assembly and patterning methods, and novel device geometries and concepts. These advances have enabled rapid growth in the development of stretchable environmental sensors. Stretchable nanocomposites based on zero-dimensional nanoparticles (NPs) [e.g., silver [Ag] NPs and gold [Au] NPs[96,97]] and flakes (e.g., micrometer-sized Ag flakes[98,99]) are compatible with various printing processes such as inkjet printing, spray printing, and nozzle printing,[100] thereby enabling low-cost, large-scale production. Nevertheless, zero-dimensional nanomaterials typically suffer from low stretchability because of their inherent low aspect ratio, as opposed to 1D NWs. Therefore, zero-dimensional NPs usually are mixed with 1D/2D materials,[101] requiring geometry engineering[102,103] or a high volume fraction to retain an electrical pathway when stretched.

One-dimensional nanomaterials, such as CNTs[46] and Ag NWs,[47,48] are probably the most prevalent constituent materials for stretchable environmental sensors. Because of the high aspect ratio of these 1D materials, when either randomly or deterministically dispersed and embedded in an elastomeric polymer matrix, they form a stretchable conductive network that can reconfigure its shape under mechanical loading. For example, Lee *et al.* fabricated very long Ag NWs in 2012 using a multiple-step growth approach; the resulting NW was over 100 μm long and had an aspect ratio over 1000.[47] Long NWs provide better stretchability than short NWs because they can form a longer percolation path and a more effective electron percolation network with a lower NW number density, which decreases the electrical resistance. If a pre-strain strategy is employed, then a very long Ag NW can achieve a stretchability of 460%.[47] Furthermore, thanks to the low percolation network associated with the high aspect ratio of the 1D shape, optically transparent stretchable sensors could be realized.

Carbon nanotubes have attracted tremendous attention in a wide range of scientific research fields since their discovery in 1991.[104] These tubes can be viewed as molecular-scale tubes formed from graphitic sheets with diameters ranging from a few nanometers to a few tens of nanometers, being semiconducting, metallic, or semimetallic depending on their chirality and diameter.[105] Because of their outstanding mechanical properties (such as high tensile strength and elastic modulus) and excellent electrical properties and chemical inertness,[106–109] CNTs have been widely used as filler materials for stretchable conductors and applied in stretchable environmental sensing devices such as light,[110] temperature,[80,111] pH,[112] and humidity sensors.[113,114] Several mixing methods (e.g., grinding,[29] jet milling,[30] and hot-rolling[101]) have been developed to obtain uniformly dispersed high-performance CNT-based stretchable conductors. In 2009, Sekitani *et al.* manufactured a printable elastic conductor composed of single-walled carbon nanotubes (SWNTs) and a fluorinated rubber.[30] The SEM image of the surface of screen-printed stretchable conductors [Fig. 3(b)] shows that the exfoliated bundles of SWNTs were dispersed uniformly in a fluorinated copolymer matrix and formed an effective conducting network, resulting in a stretchable conductor on a PDMS sheet with a conductivity on the order of 100 S cm^{-1} and a stretchability of over 100%. When the SWNT content was greater than 6% by weight, the electrical conductivity was more than 50 S cm^{-1}, while the stretchability was less than 40%. In contrast, at less than 6% of SWNTs by weight, the stretchability was higher than 50%, while the electrical conductivity was less than 40 S cm^{-1}. As it can be seen, randomly percolated CNT networks cannot obtain both high electrical conductivity and high optical transmittance simultaneously because according to the percolation theory, their short length requires a high density of CNTs to obtain high conductivity.

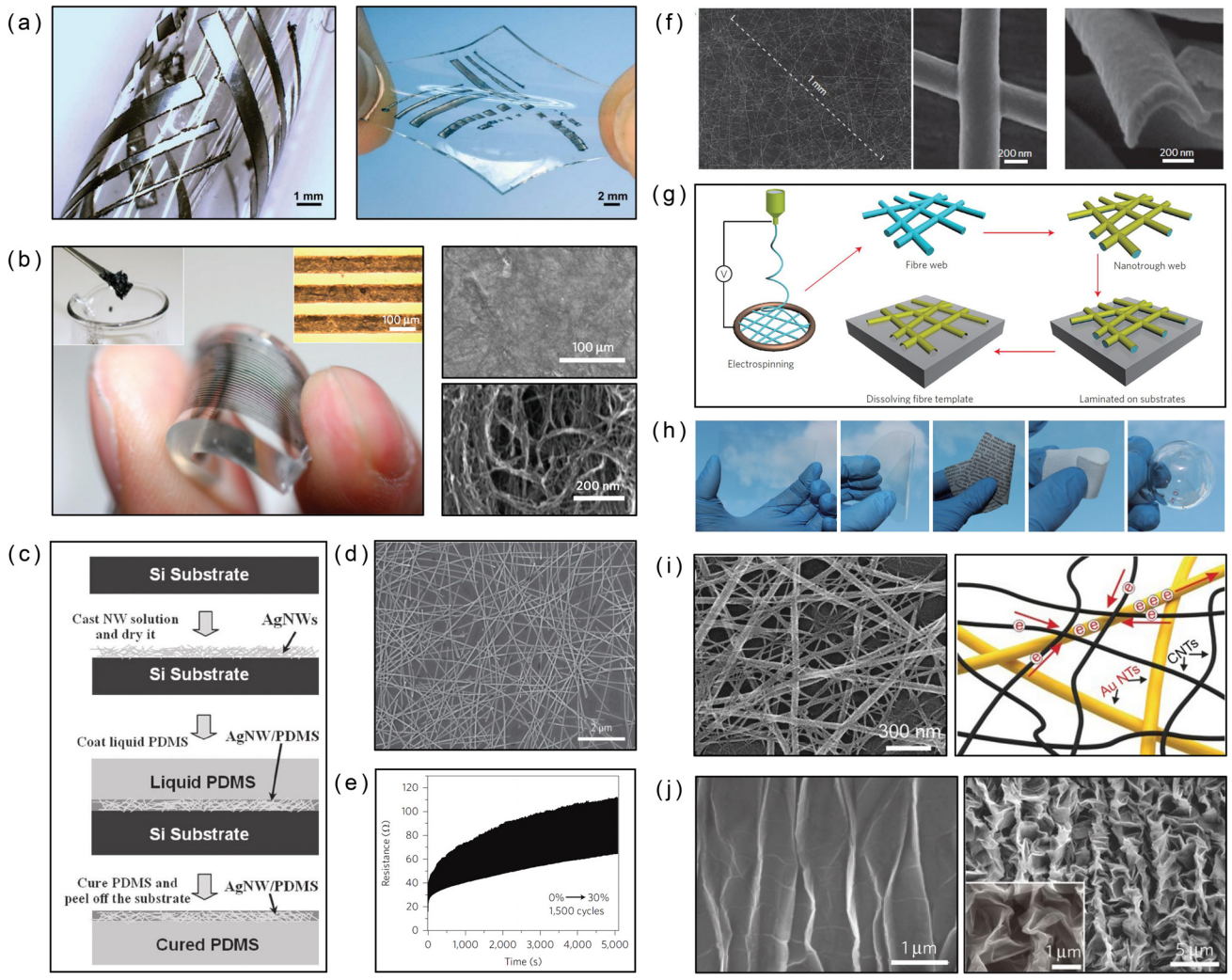

FIG. 3. Material innovation enables the development of stretchable environmental sensors. (a) Liquid metal-embedded stretchable devices.[90] Reprinted with permission from R. K. Kramer *et al.*, Adv. Funct. Mater. **23**, 5292 (2013). Copyright 2013, John Wiley and Sons. (b) Printable elastic conductors comprising SWNTs.[30] Reprinted with permission from T. Sekitani *et al.*, Nat. Mater. **8**, 494 (2009). Copyright 2009 Springer Nature. (c) A schematic showing the fabrication process of the Ag NW/PDMS stretchable conductors.[93] Reprinted with permission from F. Xu and Y. Zhu, Adv. Mater. **24**, 5117 (2012). Copyright 2012 John Wiley and Sons. (d)–(e) SEM image of the Ag NW percolation network and typical time-dependent resistance evolution of the Ag NW conductor under repeated stretching cycles.[31] Reprinted with permission from J. J. Liang *et al.*, Nat. Photonics **7**, 817 (2013). Copyright 2013 Springer Nature. (f) SEM images of Au nanotrough networks and the junction between two nanotroughs. The cross-sectional image on the right shows its concave shape.[94] (g) Schematic of the polymer-nanofiber templating process for fabricating transparent and stretchable nanotroughs.[94] (h) Au nanotrough networks can be transferred onto various substrates to produce transparent electronics.[94] Reprinted with permission from H. Wu *et al.*, Nat. Nanotechnol. **8**, 421 (2013). Copyright 2013 Springer Nature. (i) SEM image of a hierarchical percolation network of CNT-AuNT-PDMS and electrical conduction pathways.[95] Reprinted with permission from Y. L. Liu *et al.*, Angew. Chem. Int. Ed. **56**, 9454 (2017). Copyright 2017 John Wiley and Sons. (j) SEM image of the wrinkled (left) and crumpled (right) graphene sheet obtained after the pre-strained substrate is uniaxially or biaxially released.[64] Reprinted with permission from J. Zang *et al.*, Nat. Mater. **12**, 321 (2013). Copyright 2013 Springer Nature.

Randomly percolated metallic NW networks—for example, those composed of Ag NWs,[47,48] Au NWs,[115] or Cu NWs[116,117]—can simultaneously achieve high levels of optical transmittance and electrical conductivity by combining the high NW length (from several tens to over a hundred micrometers) and the high aspect ratio (from several hundred to over a thousand).[47,118] Metallic NWs have found applications in gas,[119] temperature,[120] and pH sensors.[121] Silver NWs have higher conductivity than carbon nanomaterials or any other metallic NWs.[122] In addition, Ag NWs demonstrate mechanical flexibility.[123] Furthermore, solution-based processing steps, including spray coating, drop coating, and Meyer-rod coating, allow low-cost and straightforward fabrication steps to be used to produce metallic NW based sensors. Copper NWs are other major metallic NWs that are receiving increasing interest. The conductivity of Cu is comparable to that of Ag, but Cu is 100 times less expensive and 1000 times more

abundant in nature than Ag.[117] In a typical fabrication process for an AgNW conductor [Fig. 3(c)],[93] an Ag NW solution was first deposited on a high-temperature and chemically inert temporary carrier through drop coating, spin coating, or spray coating. The as-deposited Ag NWs have a random percolation network [Fig. 3(d)].[31] After high-temperature annealing of Ag NWs to improve inter-NW junction conductivity, the Ag NW percolation network was covered with liquid-phase PDMS, followed by a 12-h curing cycle at 65 °C. The resulting composite electrode inlays in the surface layer of the PDMS are highly conductive and stretchable. A typical strain-resistance curve of the Ag NW conductor over a repeated stretching-relaxation cycle displays a quasi-reversible increase-decrease in resistance along with the stretching and relaxation of the elastomer [Fig. 3(e)].[31] A gradual but a permanent increase in both the baseline and peak resistance is seen due to breakage and rupture of the percolation network under the repeated mechanical stress. To improve the production process and further enhance electrical conductivity, the inter-NW junction has been modified using processes such as mechanical pressing, chemical modification, high-temperature annealing, and photonic sintering.[124] It is noteworthy that photonic sintering enables simultaneous reduction of the inter-NW contact resistance and direct embedding of NWs into thermoplastic elastomers attributed to light-induced extreme heat and self-limited plasmonic nanowelding locally in metallic nanostructures.[124–126] The major challenge concerning sustainable applications of Ag NWs and Cu NWs for environmental sensors is their instability against long-term electrical stress and extreme environmental conditions (e.g., the combination of high temperature and high relative humidity).[127] Even though Au NWs show excellent environmental stability, the high cost of the material prohibits their practical application.

Despite the excellent properties of metal NWs, they must be as long as possible defect-free and exhibit small junction resistance to achieve the high optical transparency (>90% T) and conductivity required for high-performance optoelectronic devices. These features are difficult to achieve concurrently. To address this challenge, Wu *et al.* proposed a strategy to obtain a deterministic mesh structure of a metal nanotrough [Fig. 3(f)].[94] They first prepared a polymer-nanofiber template by electrospinning and then coated it with metals using a standard thin-film deposition technique [Fig. 3(g)]. This technology achieves a network with a controllable structure and length for each element, enabling excellent optoelectronic performance and mechanical compliance under tension and bending [Fig. 3(h)]. Another strategy is to form a hybrid material with a hierarchical architecture,[95,128] taking advantage of properties of each material. As demonstrated by Liu *et al.*,[95] hybrid nanocomposites of CNT and Au NTs [Fig. 3(i)] showed improved electrical conductivity and mechanical stretchability because of increased effective conducting pathways between different materials. Also, metallic NWs were covered with graphene to provide protection from degradation.[128]

Because of their many outstanding and unique properties, graphene and its derivatives, graphene oxide (GO), and reduced graphene oxide (rGO) have attracted considerable attention for environmental sensing.[64,129] Graphene exhibits a combination of outstanding properties including an extremely high surface-to-volume ratio (2600 $m^2 g^{-1}$), ultrahigh electron mobility (200 000 $cm^2 V^{-1} s^{-1}$), excellent electrical conductivity (3189 S cm^{-1}), exceptionally low electronic noise, and chemical/thermal stability. Graphene-based electrochemical sensors were developed for monitoring environmental pollutants such as heavy-metal ions in aqueous solutions[130–133] and toxic gases[134] and for light sensing.[135–138] However, pristine graphene exhibits a limited stretchability of ~6%,[129] which is insufficient for most stretchable applications. Thus, a geometry-engineering approach has been incorporated to enhance its stretchability.[64,129] Kim *et al.* demonstrated a large-area patterning technique for the graphene film and explored different methods (such as a tensile pre-strain of the PDMS substrate) to enhance stretchability. However, because of the transverse strain induced by Poisson's effect, the graphene on a longitudinally pre-strained PDMS failed to show much performance improvement.[129] To prevent this problem, Kim *et al.* proposed to isotropically stretch the PDMS substrate before transferring the graphene film to it.[129] After the isotropic pre-strain was released, the graphene sheet crumpled [Fig. 3(j)].[64] Despite the fascinating properties of graphene, producing high-quality monolayer graphene involves complex, expensive, and low-yield fabrication processes, thus hampering its practical application. Therefore, rGO has been pursued as a cheaper alternative, which can be obtained from GO through chemical reduction,[139] electrochemical reduction,[140] high-temperature annealing,[141] or flash reduction.[128]

III. DEVICES AND SYSTEMS

In this section, we summarize recent advances in stretchable sensors for detecting environmental parameters including light, temperature, humidity, pH, and gases. To allow ubiquitous integration of these sensors, conformability to 3D curvilinear surfaces and stretchability to movable parts are prerequisites. Toward this end, approaches including geometry engineering, material innovations, or combinations of both have been applied.

A. Light sensors

Light is the primary essence that supports all life forms. It is a catalyst for photosynthesis in plants and provides sustenance for the survival of plankton in the oceans. On the other hand, excessive exposure to light can cause an acute and long-term effect on human health,[142] including retinal damage.[143] Too much light can also negatively affect plant photosynthesis.[144,145] Artificial night light pollution significantly affects species in the wild.[146]

Light sensors, or photodetectors (PDs), are optoelectronic devices that convert incident light or other electromagnetic radiation to an electrical signal, including light in the UV, visible, and infrared spectral regions. In addition to the optoelectronic properties of photosensitive materials, which are crucial for the performance of PDs, such as the spectral range, responsivity, ON/OFF ratio, and response time, their mechanical properties are important for achieving stretchability. Table I shows a brief overview of stretchable PDs developed over recent years,

TABLE I. Summary of the performance of the representative stretchable light sensors.

References	Materials	Strategy	Responsivity (A W^{-1})	Spectral range	ON/OFF ratio	Response time (s)	Stretchability
147	Zn_2SnO_4 NW photodiode	Material	…	UV	≈1.05 at 0% ≈1.02 at 50%	0.8	50%
148	ZnO NW photodiode	Material	…	UV	183 at 0%, 116 at 100%	≈32 at 0% ≈50 at 100%	100%
149	Electrospun SnO_2 nanowebs	Combination	…	UV	≈3 from 0 to 100%	≈12	160%
150	PbS quantum dot (QD)-P3HT hybrid NW arches	Geometry	≈800 at 365 nm, ≈100 at 625 nm, ≈3 at 850 nm	Broadband	≈30 at 365 nm, ≈50 at 625 nm, ≈4 at 850 nm	<0.58	100%
151	ZnO NR/PEDOT:PSS phototransistor	Combination	Max 86	Broadband	Max 291 at 365 nm	>10	30%
152	Wrinkled single-crystalline Ge NM	Geometry	…	Broadband	≈1.6	0.05	8.56%
110	SWNT/TiO_2 NPs	Combination	…	UV	6.2 at 0 to 200%	…	200%
153	Freestanding SiC NW fabric	Material	…	UV	…	0.03 for naked structure	50%
135	Crumpled graphene	Geometry	0.0001	Broadband	…	0.27	200%
136	Crumpled graphene/AuNPs	Geometry	0.00004	Broadband	…	…	200%
137	Rippled graphene/up-conversion nanoparticles	Geometry	∼100	Broadband	≈300	0.2 at 0%	100%

highlighting material selection, design strategies, sensor performance, and obtained stretchability.

Inorganic semiconductor materials have found prominent use in PDs, wherein their bandgap determines the operable wavelength and at which wavelength the photodetection operates most efficiently. Semiconductor PDs work on the general principle of the creation of electron-hole pairs under the action of light in photosensitive materials. When the light strikes the PD, a current is produced proportional to the intensity of the incident light. Semiconductor materials with a moderate bandgap [e.g., Si (1.14 eV) and germanium (Ge) (0.67 eV)] are most frequently used materials for photodetection because of their wide spectral range [Si (190 to 1100 nm); Ge (400 to 1700 nm)] and compatibility with semiconductor technology. To incorporate brittle semiconductor materials such as Si and Ge into stretchable PDs, geometry-engineering strategies have been adopted [Fig. 4(a)]. These strategies include transfer printing of an island-bridge device matrix onto a pre-strained elastomer,[79] using wavy topography,[152] or producing an island-bridge configuration with stretchable serpentine interconnects.[154]

Because of their direct bandgap in the UV region and a high sensitivity to UV illumination, 1D inorganic nanostructures (e.g., ZnO NWs,[148] SnO_2 NWs,[155] and Zn_2SnO_4 NWs[147]) have been used to produce stretchable UV PDs. Stemming from their large surface-to-volume ratio, the 1D nanostructure has many surface traps that can prolong the lifetime of the photocarrier;[156] furthermore, the large aspect ratio enables mechanical resilience to bending and stretching. In addition, the photosensitivity of these devices was regulated by oxygen chemisorption.[157] In 2013, Kim *et al.* reported a stretchable UV sensor produced by transferring SnO_2 NW field effect transistors (FETs) onto a radially stretched disk-shaped PDMS substrate.[155] The subsequent elastic recovery of the PDMS caused the released Au/Ti/PI substrate to exhibit a buckled structure due to compressive strain. The resulting stretchable UV sensor matrix exhibits the same sensitivity to 0.03 mW/cm^2 UV irradiation before and after 23% strain. In 2014, Yan *et al.* fabricated a highly stretchable PD by employing an intrinsically stretchable device structure with both Ag NW electrodes and ZnO NW detection channels fully embedded in an elastomer matrix.[148] The NW PD array [Fig. 4(b)] exhibited a stretchability of up to 100%. However, the device showed degraded performance with the UV current/dark current ratio changing from 188 to 116 when the tensile strain increased from 0 to 100%. In 2014, Wang *et al.* demonstrated a stretchable and transparent PD array that employed Ag NW films as the stretchable conductor and Zn_2SnO_4 NWs as the light sensing material.[147] This device performed acceptably when stretched to 50%.

Despite the greatly enhanced stretchability, reduced photo-response speed and sensitivity were observed in these PDs as a result of the fully embedded device structure, which severely impairs optoelectronic performance. As the photoresponsive behaviors of ZnO NW are related to oxygen chemisorption (i.e., photoexcitation processes associated with oxygen adsorption and desorption[148]), oxygen adsorption and desorption on the surface of the NW were significantly diminished considering the reduced oxygen level surrounding NWs in a fully embedded structure.[148] Yan *et al.* further speculated that when stretched, the lower oxygen diffusion coefficient associated with the compressed elastomer further reduced photoresponsiveness and switching time.[148] To avoid this issue, Huang *et al.* proposed a PD with an open-mesh structure in 2015.[149] The freestanding SnO_2 nanoweb [Fig. 4(c)] synthesized by electrospinning reached a stretchability of 70% and an optical transmittance of 86% at 550 nm. After transferring to a 100% pre-strained PDMS substrate, the resultant PD with both spring- and wave-like geometries could achieve stretchability up to 160%. The extraordinary stretchability was attributed to

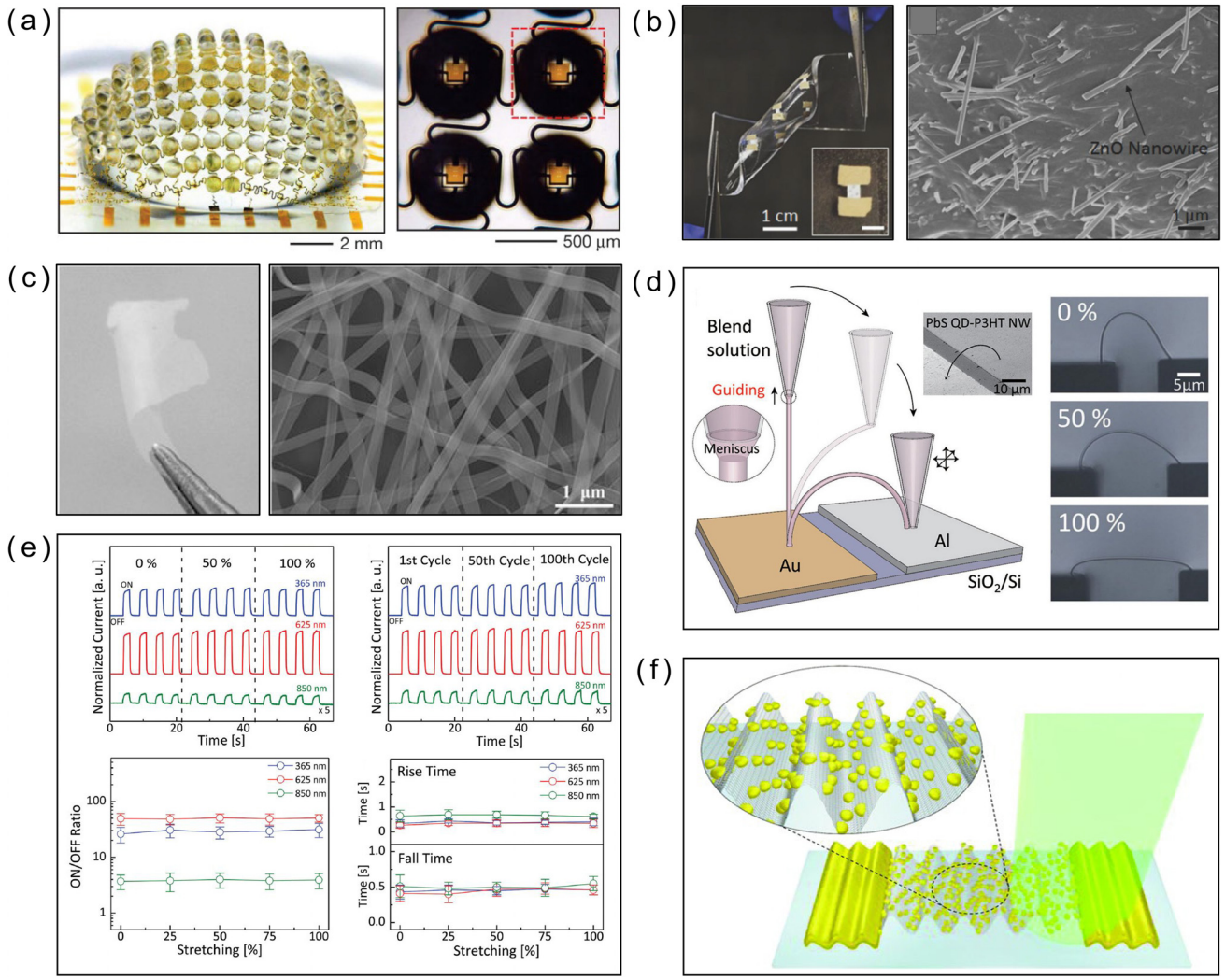

FIG. 4. Stretchable light sensors. (a) An arthropod eye-inspired 3D digital camera after hemispherical deformation; the optical micrograph shows four adjacent ommatidia in a planar format.[154] Reprinted with permission from Y. M. Song *et al.*, Nature **497**, 95 (2013). Copyright 2013 Springer Nature. (b) A stretchable NW PD array on a PDMS substrate. The SEM image shows a cross-sectional view of the ZnO NW layer embedded in PDMS.[148] Reprinted with permission from C. Yan *et al.*, Adv. Mater. **26**, 943 (2014). Copyright 2013 John Wiley and Sons. (c) Photograph and SEM image of a freestanding SnO_2 nanoweb.[149] Reprinted with permission from S. Huang *et al.*, Small **11**, 5712 (2015). Copyright 2015, John Wiley and Sons. (d) Stretchable PbS QD-P3HT hybrid NW arches obtained through direct writing by the meniscus-guided approach.[150] The inset shows an SEM image of a single NW arch on an Au–Al electrode and a series of optical microscopy images showing the NW PD stretched to 100%. Reprinted with permission from J. Yoo *et al.*, Adv. Mater. **27**, 1712 (2015). Copyright 2015 John Wiley and Sons. (e) The photo-response and ON/OFF ratios of the NW PDs for the UV-vis to near-infrared (NIR) range during repeated stretching of up to 100 cycles at 100%.[150] (f) Schematic illustrations of a stretchable PD with a crumpled graphene–Au NP hybrid structure.[136] Reprinted with permission from M. Kim *et al.*, Nanoscale **9**, 4058 (2017). Copyright 2017 the Royal Society of Chemistry.

the bendability of the nanoweb, which could withstand bending radii as small as 200 nm.[149] The UV PD showed stable optoelectronic performance (including both photosensitivity and switching speed) while remaining insensitive to strain.

NW PDs with UV-to-NIR responsiveness are emerging candidates for potential applications, such as optical communications and interconnects in nanophotonic circuits.[150] To realize UV-vis-NIR PDs, in 2015, Yoo *et al.* suggested using narrow-bandgap PbS QDs with poly(3-hexylthiophene) (P3HT) for efficient extraction and transport of photocarriers.[150] Employing a 3D direct-writing technology called the meniscus-guiding method [Fig. 4(d)],[158,159] they demonstrated for the first time stretchable NW PDs with a broad spectral range from UV to NIR. The photo-response of the freestanding hybrid NW PDs showed high sensitivity and fast response time in the UV-to-NIR range, with an ON/OFF ratio of approximately 310, 550, and 14 for 365, 550, and 14 nm, respectively. When embedded in PDMS, the 3D nanoarches of the PbS QD-P3HT hybrid NW PD array can withstand repeated stretching conditions (up to 100% strain and up to 100 cycles) [Fig. 4(e)]. The current-voltage (I-V) curves of the

NW PDs showed nearly identical behavior under stretching up to 100% or repeated stretching for up to 100 cycles. However, it should be noted that the embedded NW, compared to free-standing NW, shows a decreased photosensitivity with a reduced ON/OFF ratio of approximately 30, 50, and 4 for 365, 625, and 850 nm, respectively.

Graphene-based PDs have attracted intense interest for their exceptional properties such as outstanding mechanical strength, extraordinary carrier mobility, broadband absorption from the UV to the terahertz regions, and fast response speeds. Nevertheless, further applications of graphene to stretchable and highly sensitive PDs have been hampered by limited intrinsic stretchability and photoabsorption efficiency.[160] To address these challenges, various hybrid graphene architectures comprising photonic or plasmonic nanostructures (e.g., metal nanoparticles or colloidal quantum dots, wherein nanoscale phenomena such as quantum confinement and plasmonic effects play a principal role) were introduced to improve photoresponsivity, combined with geometry engineering to enhance flexibility and stretchability. As an example, Kang *et al.* proposed a crumpled graphene PD with a stretchability of 200% in 2016.[135] Such a crumpled graphene allowed not only improved stretchability but also increased optical absorption ascribed by areal densification of graphene. In 2017, Kim *et al.* from the same group fabricated a crumpled PD based on the graphene/AuNP composite [Fig. 4(f)], taking advantage of the plasmonic enhancement by Au NPs.[136] By doping crumpled graphene with light-harvesting perovskite $CH_3NH_3PbI_3$ microwires, Ding *et al.* achieved a stretchable PD with a fast response time of less than 0.12 s under 100% tensile strain in 2018.[138] However, all the above-mentioned graphene PDs showed low photoresponsivity of less than 1 mA W^{-1}. In 2018, Kataria *et al.* achieved a broadband PD employing graphene and broadband photo-responsive up-conversion nanoparticles with a stretchability of 100%, a response time of less than 200 ms, as well as a photoresponsivity of about 100 AW^{-1}.[137]

B. Temperature sensors

Temperature is a fundamental parameter that is not only important for the health and growth of life (humans, animals, and plants) and migration patterns and habits of marine animals[161] but also crucial for the operation of sensors, instruments, and other electronic devices because most of them are highly temperature dependent. Stretchable temperature sensors could be worn on the human body or on robots to detect environmental temperature, send feedback for calibrations, and issue early warnings to prevent damage to thermally sensitive electronics. Notwithstanding the challenging mechanical requirements of producing highly flexible and stretchable sensors, their performance should not be compromised compared to their conventional rigid counterparts. This new class of sensor requires a wide detection range (−10 to +85 °C), reasonable response speed, and acceptable sensitivity (1.0 °C or lower). If biological species, such as humans, animals, or plants, are the measurands, a lower temperature range of interest would be acceptable, but higher sensitivity would be required.[162]

Stretchable temperature sensors have been realized through either material or geometry innovations or through a combination of the two approaches. A summary of stretchable temperature sensors that have been developed in recent years, highlighting the material choices, design strategies to achieve stretchability, sensing mechanisms, sensor performance, and maximum reported stretchability, is provided in Table II. Because of its simplicity in implementation and high sensitivity, the thermoresistive effect is the primary sensing mechanism used in stretchable temperature sensors.[163] The thermoresistive effect, in which the resistivity of a material exhibits a temperature dependency, arises from the thermally induced change of the number of charge carriers, their mobility, and the scattering effect of lattice vibrations.[163] The pyroelectric effect (e.g., ZnO NWs),[164] thermoelectric effect (e.g., Si nanostructures),[81] and thermochromic effect (e.g., polydiacetylenes)[165] have also been used as the technical bases for stretchable temperature sensors.

Earlier work focused on producing a stretchable temperature sensor from conventional thermoresistive materials through geometrically engineering the sensing materials into buckled thin films,[166] serpentines, or meander traces.[173] For example, mechanically flexible but non-stretchable thin-film materials were attached to the pre-strained PDMS substrate

TABLE II. Summary of the performance of the representative stretchable temperature sensors.

References	Materials	Strategy	Sensing mechanism	Sensitivity	Range (°C)	Stretchability
166	Buckled thin film	Geometry	Thermoresistive	…	20–110	30%
167	Serpentine-shaped Au film	Geometry	Thermoresistive	0.002778 $°C^{-1}$	0–23	…
81	Serpentine-shaped single-crystalline silicon nanoribbon	Geometry	Thermoelectric	≈−0.003V $°C^{-1}$	27–55	10%
169	Coiled polypyrrole (PPy)-coated threads	Geometry	Thermoresistive	…	35–95	100%
111	SWNT/thermo-responsive polymer	Material	Thermoresistive	…	0–80	70%
170	Graphene nanowall/PDMS	Material	Thermoresistive	0.214 $°C^{-1}$	25–120	…
171	rGO/PU	Material	Thermoresistive	1.34% $°C^{-1}$	30–80	70%
80	Polyaniline (PANI) nanofiber with CNT thin-film transistors	Material	Thermoresistive	1.0% $°C^{-1}$	15–45	30%
172	Polyacrylamide/carrageenan hydrogels	Material	Thermoresistive	2.6% $°C^{-1}$ at 200%	25–92	330%
164	ZnO NW/PU fiber	Material	Pyroelectric	16.8% $°C^{-1}$ at 100 °C	25–55	150%
165	PDMS/polydiacetylenes	Material	Thermochromic	…	25–85	300%
168	Crumpled graphene/PDMS	Combination	Thermoresistive	−2.11 $°C^{-1}$ at 50% strain	30–100	50%
120	Cu NW mesh	Combination	Thermoresistive	7 Ω $°C^{-1}$	RT-48	80%

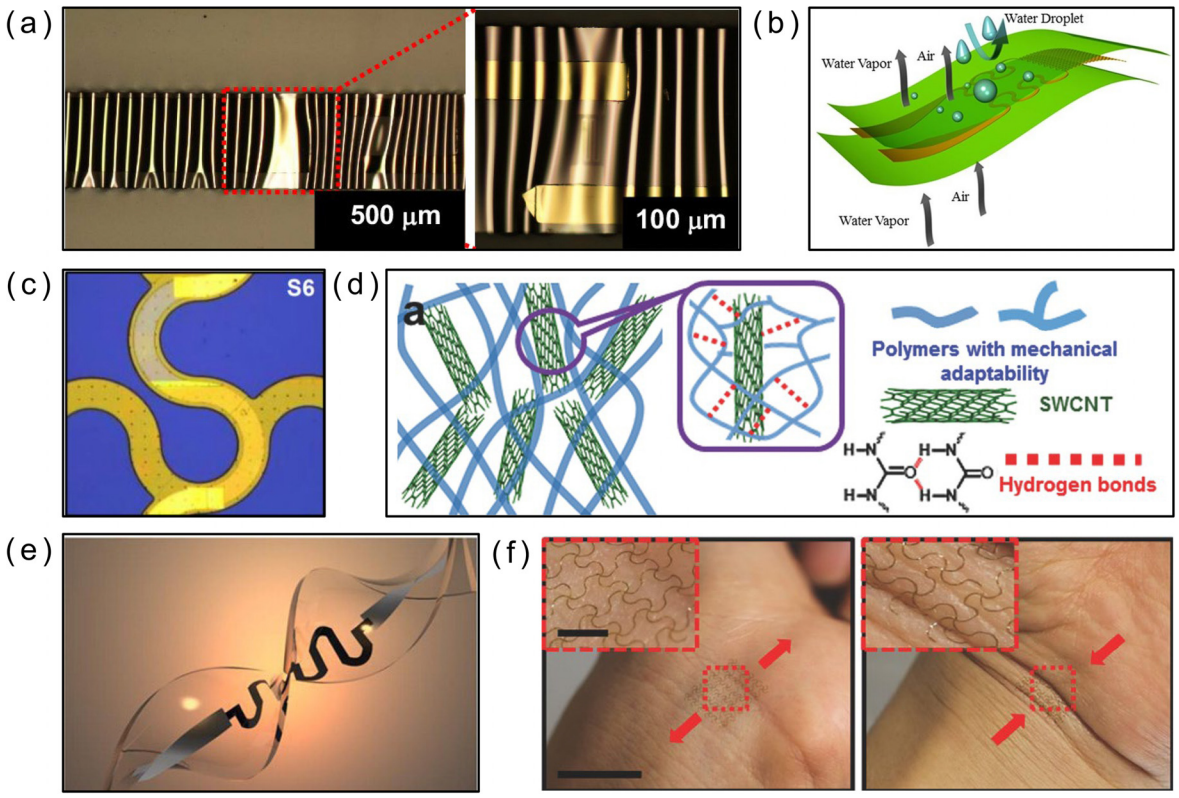

FIG. 5. Stretchable temperature sensors. (a) Stretchable temperature sensor above a PDMS substrate with buckled patterns.[166] Reprinted with permission from C. J. Yu *et al.*, Appl. Phys. Lett. **95**, 141912 (2009). Copyright 2009 AIP Publishing. (b) Conceptual illustration of a waterproof and vapor-permeable temperature sensor.[167] Reprinted with permission from Y. Chen *et al.*, Sci. Rep. **5**, 11505 (2015). Copyright 2015 Author(s) licensed under a Creative Commons Attribution 4.0 International License. (c) Microscopic images of serpentine-shaped silicon nanoribbon p-n junction diodes for the temperature sensor.[81] Reprinted with permission from J. Kim *et al.*, Nat. Commun. **5**, 5747 (2014). Copyright 2014 Author(s) licensed under a Creative Commons Attribution 4.0 International License. (d) Schematic illustration of soft and stretchable thermo-responsive materials based on hydrogen bonds. The blue lines refer to the randomly branched network composed of polymers, and the red lines refer to hydrogen bonds in the polymer.[111] Reprinted with permission from H. Yang *et al.*, Adv. Mater. **28**, 9175 (2016). Copyright 2016 John Wiley and Sons. (e) Photograph of the stretchable graphene thermistors in twisted states.[168] Reprinted with permission from C. Yan *et al.*, ACS Nano **9**, 2130 (2015). Copyright 2015 American Chemical Society. (f) Photographs of the Cu NW mesh integrated onto the skin of the wrist under stretch (left) and compression (right).[120] Reprinted with permission from S. Han *et al.*, Adv. Mater. **28**, 10257 (2016).

and formed an out-of-plane periodically buckled pattern after relaxation of pre-strain [Fig. 5(a)].[166] The resulting device shows a broad measurement range (20 to 110 °C) and a stretchability of 30% coupled with decent sensitivity. A waterproof, vapor-permeable, biocompatible, and stretchable temperature sensor was fabricated [Fig. 5(b)].[167] An Au sensing film was patterned into an in-plane S-shape to achieve stretchability and then packaged in the neutral plane of a 3D laminate that helps minimize further strain caused by the bending deformation. To be biocompatible, a semipermeable PU-based porous film was used as the encapsulation material, making it possible to adhere to the human body while maintaining its stretchability. Kim *et al.* carried out a more comprehensive performance study of the stretchable temperature sensor based on the in-plane serpentine design [Fig. 5(c)].[81] Current-voltage curves of single-crystalline Si nanoribbon-based temperature sensors at room temperature over applied strain show that the divergence between each I-V curve under different strains was markedly mitigated as the curvature of sensors increased. The large curvature of the sensors allows for repeatable temperature measurements with the minimal effect of mechanical deformations or pressure on the temperature sensing. He *et al.* demonstrated another geometry-engineered stretchable temperature sensor.[169] They developed a continuous large-scale dyeing process to grow polypyrrole (PPy) as the sensing element on the Dacron thread. The resulting thread was then wound on an elastic PU fiber into a coiled structure. This 3D structure could endure tensile strain over 100% without destroying the electrical conducting performance of PPy. Geometry-engineered temperature sensors usually show consistent sensitivity under different applied strains as the microscopic structure of the materials remains nearly unchanged. Nevertheless, they are mostly limited to a lower maximum stretchability.

Recent studies have focused on the thermoresistive effect in carbon nanomaterials including CNTs[111] and graphene for temperature sensors.[168] Nevertheless, thermal resistivity of these materials is relatively low compared to more conventional materials. For example, their temperature coefficient of

resistance values typically is lower than 1250 ppm/K compared to several thousands to several tens of thousands of ppm/K for metals or bulk semiconductors.[174] To improve the thermo-sensitivity of these materials, they have been mixed with other materials to form a hybrid sensitive material. A soft temperature sensitive nanocomposite was fabricated by doping mechanically adaptable polymers based on hydrogen bonds with SWNTs [Fig. 5(d)].[111] The weight ratio of SWNTs to polymers markedly influenced the mechanical adaptability, electrical conductivity, and thermo-sensitivity of the material. Moreover, a combination of material synthesis and geometry-engineering strategies could lead to a more effective temperature sensor. For example, a stretchable graphene thermistor with a stretchability up to 50% has been fabricated [Fig. 5(e)].[168] In that device, lithographically filtrated 3D crumpled graphene channels in a serpentine shape and highly conductive and stretchable Ag NW electrodes were fully embedded in a PDMS matrix to achieve excellent stretchability. Nevertheless, the device demonstrated strain-dependent thermo-sensitivity. Also, a stretchable NW percolation network film was photo-lithographically patterned and dry etched in a filamentary serpentine trace mesh, which allowed it to minimize the induced strain experienced by the NWs during large deformation when stretched.[120] The fabricated Cu NW mesh was placed on the wrist and maintained a highly intimate contact with the skin even when completely stretched and compressed [Fig. 5(f)]. The results showed that the structure could be stretched reversibly up to 80% without noticeable plastic deformation or fractures, as opposed to a traditional Cu thin-film-embedded structure that fractures at a strain of 55% when the local strain exceeds the fracture limit (~12%).

As reported by Liao *et al.* in 2016,[164] a pyroelectric temperature sensor with a stretchability of 150% was achieved based on ZnO NWs with PU fibers. In that device, stretchable PU fibers function as the skeleton of the sensor to provide mechanical adaptability. ZnO NWs as the sensitive material were coated over this skeleton. However, the temperature sensitivity of the ZnO NW@PU fiber sensors decreased from the initial value of 39.3% $^{\circ}C^{-1}$ to 16.8% $^{\circ}C^{-1}$ at 100% tensile strain. The thermally induced polarization electric field and charge separation within the ZnO NWs result in the generation of pyroelectric current. Upon stretching, the PU fibers were brought closer to each other, causing a restricted thermal expansion of ZnO NWs. Therefore, the current variation was reduced, and so, the sensitivity of the sensor decreased under strain loading.

C. Humidity sensors

Humidity is a critical parameter in determining the geographical distribution and the maximum intensity of precipitation, biospheric, and surface hydrology and significantly affects the operation of electronics.[175] Human or animal life dependent on perspiration to regulate internal body temperature, high humidity, and ambient temperature impair heat exchange efficiency through sweating and heat conduction. Consequently, these conditions lead to heat stress and contribute to enhanced morbidity and mortality.[176] Conversely, low humidity has also adverse effects on human health.[177] Measurements of the humidity or moisture level in the environment or human skin could, therefore, be beneficial in evaluating a variety of physiological and metabolic conditions and further help elucidate growth, repair, and aging mechanisms. Table III presents a brief overview of stretchable humidity sensors developed over recent years, highlighting the material selection, design strategies, sensor mechanisms and performance, and stretchability obtained. The most commonly used humidity sensor measures relative humidity, which is the ratio of the amount of moisture content in air to the saturated moisture level that air can hold at a given temperature and pressure level.[178] Humidity sensors are also categorized in terms of the type of sensing material used, which include ceramic, semiconductor, and polymer types. According to sensing mechanisms, humidity sensors are divided into resistive type and capacitive type. These sensors use changes in their conductivity or permittivity of the hygroscopic sensing materials when exposed to the humid environment due to adsorption and desorption of water vapor molecules.

Figure 6(a) shows a capacitive-type humidity sensor consisting of intrinsically stretchable CNT micro-yarn circuitry incorporated with an Ecoflex film onto the PDMS substrate.[113] The sensor configuration is nothing more than a parallel plate capacitor, consisting of a dielectric layer sandwiched between two conductor layers. The hierarchical CNT nanostructure has outstanding fatigue resistance and damage tolerance under external stress, thereby providing sensor devices with high

TABLE III. Summary of the performance of the representative stretchable humidity sensors.

References	Materials	Strategy	Sensing mechanism	Sensitivity	Response time	Range	Stretchability
81	PI	Geometry	Capacitive	0.08% %$^{-1}$	≈200 s	15–60%	…
68	Wrinkled PANI film	Geometry	Resistive	…	…	11–95%	40%
179	3D ordered molybdenum disulfide (MoS_2)	Geometry	Resistive	…	…	30–90%	50%
180	PANI composite fiber	Geometry	Resistive	~200 MΩ–2 MΩ between 20 and 90%	≈400 s	20–90%	200%
181	Wrinkled 2D WS_2 film	Geometry	Resistive	R0/R = 2357 from 20 to 90%	A few seconds	20–90%	40%
92	Liquid metal and ionic liquid	Material	Both	…	≈1 h	13–60%	…
182	GO	Material	Capacitive	0.15–4.27 for 20–90% relative humidity	≈30 s	30–90%	3%
113	CNT yarn/Ecoflex	Material	Capacitive	0–0.025 for 48–70%	…	48–75%	…
114	CNT/poly(vinyl alcohol) (PVA)	Material	Resistive	0–20 for 60–100% relative humidity	40 s	60–100%	160%
183	rGO/PU	Material	Resistive	0.13% %$^{-1}$	A few seconds	0–70%	60%
184	Poly-MMA-MAPTAC/conductive yarns	Material	Capacitive	0.0369	35 s	20–90%	3%

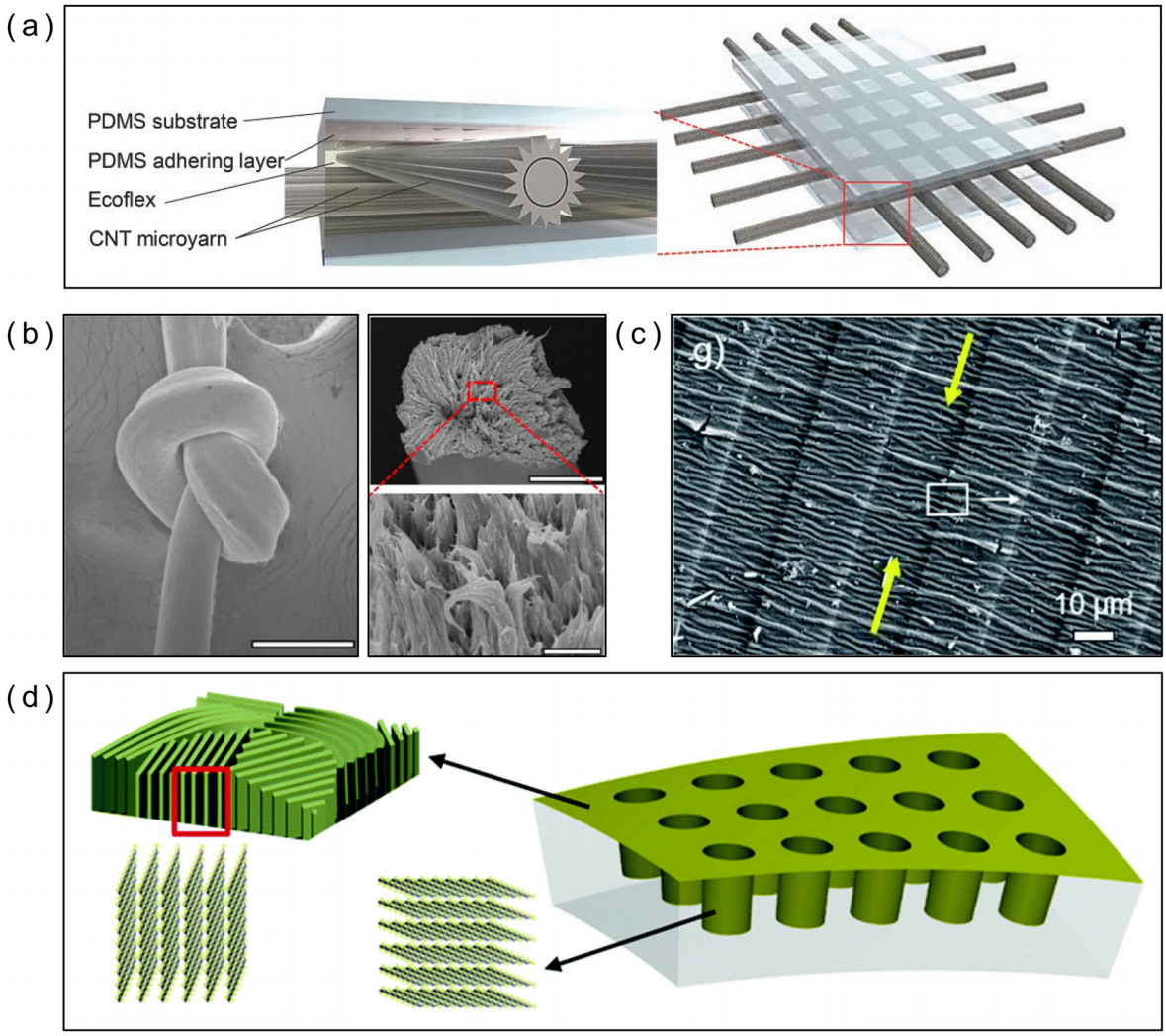

FIG. 6. Stretchable humidity sensors. (a) Schematic view of the active layers of the CNT micro-yarn-based capacitive humidity sensor cell.[113] Reprinted with permission from S. Y. Kim *et al.*, Adv. Mater. **27**, 4178 (2015). Copyright 2015 John Wiley and Sons. (b) SEM images of tightly knotted SWNT/PVA filaments for resistive humidity sensors and high-magnification, cross-sectional morphologies of the filaments. The scale bars are 100, 20, and 1 μm, respectively.[114] Reprinted with permission from G. Zhou *et al.*, ACS Appl. Mater. Interfaces **9**, 4788 (2017). Copyright 2017 American Chemical Society. (c) Nanostructured PANI wrinkle on the micro-grooved PDMS substrate.[68] Reprinted with permission from H. Ryu *et al.*, RSC Adv. **4**, 39767 (2014). Copyright 2014 Royal Society of Chemistry. (d) Schematic illustration of the large-area integration of 3D ordered 2D MoS_2 vertical layers onto a flexible PDMS substrate enabled by a water-assisted layer transfer method.[179] Reprinted with permission from M. A. Islam *et al.*, Nanoscale **10**(37), 17525–17533 (2018). Copyright 2018 Royal Society of Chemistry.

reliability and stretchability. With a change in humidity, the water molecules are absorbed/desorbed by the hygroscopic dielectric materials, which changes the dielectric constant and thus the measured capacitance. Figure 6(b) shows a tightly knotted resistive-type humidity sensor based on SWNT/PVA filaments.[114] Because of the hygroscopicity of environmentally friendly PVA, the diameter of the SWNT/PVA filament under wet conditions can be twice as much as under dry conditions, thereby changing the electrical resistance of the SWNT network.

To promote the sensitivity, selectivity, and chemical and thermal stabilities of a humidity sensor, intensive efforts have been focused on the exploration of humidity-sensitive nanostructured materials, including CNTs,[114] MoS_2,[179] WS_2,[181] GO,[182] and PANI.[68] In 2014, Ryu *et al.* fabricated a nanostructured PANI sensing film and coated it on a pre-strained PDMS substrate [Fig. 6(c)].[68] The PDMS substrate incorporated a micro-grooved structure, which effectively prevented cracking induced by the Poisson effect in the direction perpendicular to the stretching direction. The resulting humidity sensor with a periodic wrinkled structure could be stretched up to 40%. A spiral configuration was used in a more recent study to fabricate a humidity sensor with an ultra-stretchability of 200%.[180] This resistive-type humidity sensor consists of a highly stretchable composite

fiber with spandex-covered yarn coated with humidity-sensitive nanostructured PANI through a solution process. The variation of electrical conductivity depending on the absorption and desorption of water provides the humidity sensitivity of PANI. Thanks to the spiral configuration of the spandex-covered yarn, no actual elongation of the conducting polymers took place during stretching, thereby preserving the humidity sensitivity at different strain levels.

In recent years, 2D materials have gained increasing popularity for use in humidity and gas sensors. These materials provide decent sensitivity to absorbed molecular species due to almost total exposure of all their atoms from the 2D configuration. In particular, a GO-based humidity sensor has achieved an unprecedented response and a recovery time of 30 ms.[185] The interaction of GO with water molecules is particularly interesting because in addition to its extremely large surface area and the observed superpermeability to water, GO surface functional groups react with water molecules, giving rise to protonation and an increase in the density of charge carriers.[185] A GO film as the active sensing material was spray coated on a patterned graphene channel for humidity sensing. However, this capacitive humidity sensor can only be stretched to 3%.[182] Several strategies were proposed to improve the mechanical flexibility and stretchability of 2D-material-based humidity sensors. In 2017, Trung *et al.* employed rGO and mixed with PU to fabricate a transparent humidity sensor.[183] This device exhibits impressive response and relaxation times of 3.5 and 7 s, respectively. The sensor features a 200-nm-thick rGO/PU composite sensing layer with an rGO of 10% by weight, combined with an optical transmittance of 78%. Noteworthily, the author demonstrated that the sensitivity and the response and recovery times of the device for humidity sensing remain almost unchanged after stretching up to a strain of 60% or after 10 000 stretching cycles at 40% strain. The sensing mechanism is possibly due to both the conductive rGO filler and the elastomeric PU matrix: rGO nanosheets have high surface/volume ratios and possess a large density of surface defects and hydrophilic functional groups, including the OH and COOH groups. Furthermore, PU also contains hydrophilic functional groups such as NH and CO groups, which facilitates water molecule intake from the environment. Moreover, the water molecules absorbed into the rGO/PU composite film may cause swelling, which significantly increases the distance between the nanosheet-nanosheet junction and aggravates the degree of discontinuity in the rGO/PU nanocomposites, thus increasing the electrical resistance of the sensor. In 2017, Guo *et al.* synthesized large-area polycrystalline WS_2 few-layer films by metal sulfurization, which were transferred to a pre-strained PDMS substrate for the stretchable humidity sensor.[181] The few-layer WS_2 humidity sensor showed a fast response (5 s) and recovery time (6 s) and exhibited a decrease in electrical resistance at increasing humidity, which may be attributed to the intrinsic hydrophobic nature of the WS_2 film. Furthermore, thanks to the atomically thin WS_2 film, the device is optically transparent (80% at 550 nm) and flexible enough to be attached to curvilinear surfaces. The humidity response shows little dependency on the applied strain of the device, which is a noteworthy property. In 2018, Islam *et al.* grew and transferred vertically aligned MoS_2 layers and then integrated them in a PDMS substrate with a 3D ordered pillar array [Fig. 6(d)].[179] The new form of 2D materials exhibits an improved sensitivity for water molecule detection compared to conventional horizontally aligned 2D MoS_2 layers even under significant mechanical bending. The device demonstrates a stretchability to 50%, while retaining its structural integrity upon repeated stretching-relaxing cycles. The surface-exposed 2D edge layer sites of both the vertically oriented 2D MoS_2 layers and the 3D PDMS pillar enhanced the surface area of the materials, increasing the surface area by five times over non-patterned samples, which drastically increased the area of the active sites for water molecule capture.

D. pH sensors

A logarithmic scale used to specify the hydrogen ion activity in water-based solution, indicating its acidity or alkalinity, is referred to as pH. pH is considered a fundamental environmental signal, and monitoring pH in our environment is of vital importance. For example, fluctuations in ocean pH are expected to have a massive impact on the physiological resilience in marine organisms.[186] Acid rain, excessive human activities, and untreated sewage can cause environmental pH changes and the acidification of soils, streams, lakes, and seawater,[187] which would pollute our drinking water and destroy the living environment for marine animals.

The potentiometric pH sensor represents a major class of pH sensing techniques. Fundamentally, a potentiometric pH sensor consists of an ion sensitive electrode (ISE) and a reference electrode, both of which are attached to a voltmeter. The potential difference between these electrodes, when they are immersed in a solution, is proportional to the pH value. Because ISEs respond selectively to ions in the presence of others, it is usually considered directly related to the activity of H_3O^+ in aqueous solutions. Because of the straightforward transduction principle and simple readout configuration, potentiometric pH sensors have been the dominant instrument used for pH sensing, including stretchable pH sensors.[112,121,188] The spectrometric pH sensor is an alternative sensing technique. Unlike electrochemical pH sensing, the spectrometric technique indirectly acquires the pH of a solution by measuring the concentration of the acidic and basic forms of the pH indicators.[189] For example, a stretchable optoelectronic sensor system coated with a pH-sensitive organically modified silica film was developed.[190] The UV-vis absorption intensity of the pH-sensitive film decreases as pH increases. The measurement is based on the principle that by using a PD to measure the light intensity passing through the pH-sensitive film, we can quantitatively derive the pH.

To date, the most frequently used ISE material for potentiometric pH sensors is a glass membrane, which has the disadvantages of being delicate, expensive, and rigid. With the goal of realizing stretchable pH sensors, novel stretchable pH-sensitive materials along with device structures are being exploited. PANI, known as a pH-sensitive conducting polymer, has received increasing attention as an ISE material for wearable, stretchable pH sensors because of its low cytotoxicity and low skin irritation.[112] On the other hand, accounting for the compatibility with

semiconductor device manufacturing processes, solid-state metal oxides, particularly iridium oxide, are considered to be a particularly advantageous ISE material. It has also other favorable properties such as high sensitivity (super-Nernstian responses to pH change), stability over a wide pH range, rapid response time, minimal potential drift, outstanding chemical selectivity, and high durability.[191] Nevertheless, iridium oxide is not stretchable. A brief overview of stretchable pH sensors developed over recent years is listed in Table IV, highlighting material selection, design strategies, sensor mechanisms and performance, and obtained stretchability.

Non-stretchable ISE materials were optimized through geometry engineering into meander/serpentine patterns and island-bridge configurations to produce stretchable pH sensors.[121,188] In 2014, Chung *et al.* reported an island-bridge strategy enabled stretchable pH sensor array.[191] In 2015, Hwang *et al.* reported the production of stretchable Si NM- and Si NR-based transient electronics with device islands connected by serpentine or out-out-plane interconnects that allow the system to accommodate large deformations without fracture.[82] In a doped Si NRs-based pH sensor array [Fig. 7(a)],[82] the stretchable interconnect undergoes in- and out-of-plane buckling in response to tensile loads, whereas the islands do not deform, thus remaining flat. When the device is exposed to solutions with different pH values, changes in conductance of devices were measured. Here, the $-NH_2$ and −SiOH groups on the functionalized surfaces of the Si NRs undergo protonation to $-NH_3^+$ at low pH and deprotonation to $-SiO^-$ at high pH.

In 2017, Rahimi *et al.* introduced a low-cost technique to fabricate a highly stretchable electrochemical pH sensor.[188] The stretchable conductive interconnection consists of porous carbonized 2D serpentine traces fabricated by direct laser carbonizing and micromachining of a PI sheet bonded to an Ecoflex substrate [Fig. 7(b)]. These carbonized 2D serpentine traces were subsequently permeated with PANI as the conductive filler, binding material, and pH-sensitive membrane. The sensor was able to withstand longitudinal and transverse elongations of up to 100% in different pH buffer solutions with a minimal deviation of less than ±4 mV. The ultimate elongation of this device is 135%. In 2018, Oh *et al.* fabricated a PANI-based skin-attachable and stretchable electrochemical sensor that can detect pH in human perspiration.[112] A percolation network of Au nanosheets (Au NS) and CNTs was formed via vacuum filtering and a layer-by-layer method, respectively, on a stretchable substrate [Fig. 7(c)] as the stretchable interconnect for the PANI working electrode and the Ag/AgCl reference electrode. The fabricated electrodes were further encapsulated in silbione. The electrochemical performance of the fabricated PANI-based pH sensor was analyzed at room temperature [Fig. 7(d)]. Detection of pH was carried out by measuring the open-circuit potential as pH was varied from 4 to 8 using the standard buffer solution. The sensor exhibits a flat curve at a constant pH value, and the change in open-circuit potential with pH was used to obtain the linear regression curve. The slope of the calibration was used to estimate the sensitivity of the sensor. The device showed highly selective sensitivity to pH against other ions, including Cu^{2+}, NH^{4+}, K^+, and Na^+. This sensor retains its selectivity and sensitivity at different strain levels and without degradation under repetitive deformations of 30% strain over 1000 cycles. To further enhance the stretchability, PANI-based stretchable pH-sensitive materials were patterned into a serpentine/meander shape. In 2018, Xuan *et al.* fabricated a stretchable electrochemical pH sensor consisting of an electrodeposited PANI membrane and cast Ag/AgCl on a LIG/Ag NW/PDMS stretchable electrode.[121] The Ag NW percolation network layer was introduced to reduce the sheet resistance of the electrode and enable the stretchability. The serpentine filamentary pattern further enhances stretchability, with a minimal resistance change under strain up to 40%.

Highly stretchable, biocompatible pH-sensitive hydrogels have been developed for biological and biomimetic applications,[192,194] which is otherwise not possible for a geometry-engineered stretchable pH sensor. For example, highly stretchable, tough, and pH-sensitive agar/P(AM-*co*-AA) interpenetrating polymer network hydrogels were successfully prepared,[192] which exhibit reversible swelling and recoverable deformation against the pH of media. A soft and robust hydrogel-based pH sensor was fabricated via 3D printing of poly(styrenesulfonate) doped poly-(3,4-ethylenedioxythiophene) with hydrophilic polyurethane (PEDOT:PSS/HPU) inks [Fig. 7(e)],[192] wherein conductive PEDOT:PSS provides the pH sensitivity, and HPU acts as a reinforcing matrix and prevents PEDOT:PSS from dissolving. The resistance of this hydrogel depends on both the pH and the degree of swelling. For a fully swollen hydrogel, a linear correlation between conductivity and the pH was observed.

TABLE IV. Summary of the performance of the representative stretchable pH sensors.

References	Materials	Strategy	Sensing mechanism	Sensitivity	Range	Stretchability
190	Silicate (organically modified silica) film	Geometry	Optical	4.42 mV pH^{-1}	4–8	35%
112	PANI/CNT/AuNS working electrode Ag/AgCl/AuNS reference electrode	Materials	Electrochemical	71.44 mV pH^{-1}	4–8	30%
121	PANI-laser-induced graphene (LIG)-Ag NW-PDMS Ag/AgCl-LIG-Ag NW-PDMS	Combination	Electrochemical	56 mV pH^{-1}	4–7	40%
188	Serpentine PANI/C-PI	Combination	Electrochemical	−53 mV pH^{-1}	4–10	135%
82	Doped Si NR functionalized with APTES	Geometry	Electrochemical	0.1 ± 0.01 μS pH^{-1} or 0.3 ± 0.02 μS pH^{-1}	3–10	30%
191	Iridium oxide	Geometry	Electrochemical	69.9 ± 2.2 mV pH^{-1}	4–10	…
192	PEDOT:PSS/HPU hydrogels	Materials	Electrochemical	…	3–13	50%
193	Graphite/PU electrode Ag/AgCl	Geometry	Electrochemical	11.13 mV pH^{-1}	5–9	53%

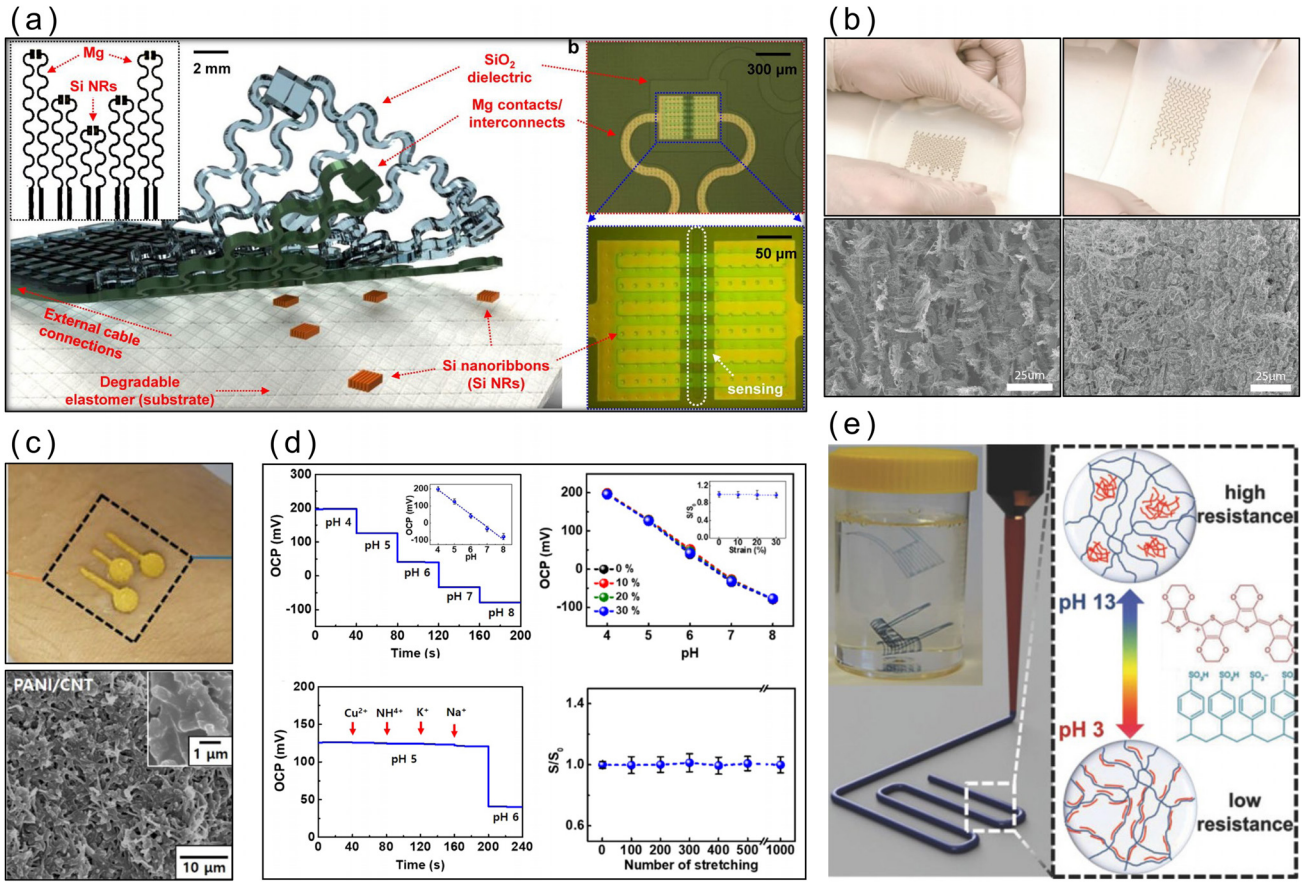

FIG. 7. Stretchable pH sensors. (a) Exploded view schematic illustration of a biodegradable, stretchable pH sensor array based on doped Si NRs. Optical microscopy images on the right show an individual pH sensor and its magnified view.[82] Reprinted with permission from S. W. Hwang *et al.*, Nano Lett. **15**, 2801 (2015). Copyright 2015 American Chemical Society. (b) A stretchable pH sensor array based on the PANI/C-PI nanocomposite. The SEM images show pristine porous laser-carbonized PI and the PANI/C–PI composite.[188] Reprinted with permission from R. Rahimi *et al.*, ACS Appl. Mater. Interfaces **9**, 9015 (2017). Copyright 2017 American Chemical Society. (c) A stretchable and skin-attachable electrochemical pH sensor based on PANI/CNT nanocomposites. The SEM image shows the surface morphology of the PANI/CNT film.[112] Reprinted with permission from S. Y. Oh *et al.*, ACS Appl. Mater. Interfaces **10**, 13729 (2018). Copyright 2018 American Chemical Society. (d) Electrochemical performance (sensitivity, selectivity, and stability) of the pH sensor employing PANI/CNT nanocomposites under different mechanical loading conditions.[112] (e) 3D printed hydrogel-based pH sensors employing pH-sensitive PEDOT and hydrophilic polyurethanes.[192] Reprinted with permission from S. Naficy *et al.*, Adv. Mater. Technol. **3**, 1800137 (2018). Copyright 2018 John Wiley and Sons.

E. Gas sensors

Monitoring of air quality and toxic industrial gases such as carbon monoxide, oxides of nitrogen, and ammonia (NH_3) has become increasingly important over the last decade. Long-term exposure to air pollution, mostly by $PM_{2.5}$, has led to 3.3 million premature deaths per year worldwide,[195] predominantly in Asian countries such as China and India. Air pollution has a significant impact on the climate and the environment, jeopardizing global agricultural and natural ecosystems.[196]

A brief overview of stretchable gas sensors that were developed over recent years is listed in Table V, highlighting material selection, design strategies, analytes, sensor performance, and obtained stretchability.

Three device structures, relying on the direct chemical interaction between the sensing material and the analyte, were demonstrated for stretchable gas sensors: (1) chemiresistors (2) FET-based gas sensors, and (3) triboelectric-generator-based gas sensors. The chemiresistor gas sensor is usually constructed using materials that change their electrical resistance in response to changes in the nearby chemical environment. For example, Gutruf *et al.* reported on a ZnO-based stretchable and transparent chemiresistor in 2015.[198] Here, the unique microtectonic structure [Fig. 8(a)] of the functional ZnO films resulted in enhanced sensing performance for the device. The room temperature response of this device [Fig. 8(b)] shows an apparent response to both H_2 and NO_2. The mechanism of gas interaction with the sensing material is primarily governed by the chemical properties of each material. H_2 is a reducing gas, and hence, the resistance of ZnO decreases upon exposure to H_2. On the other hand, a reaction with an oxidizing gas such as NO_2 would cause

TABLE V. Summary of the performance of the representative stretchable gas sensors.

References	Materials	Strategy	Analyte	Sensitivity	Range	Stretchability
197	PANI/MoS_2	Combination	NH_3	2.513 ppm^{-1}	0.05–30 ppm	30%
198	ZnO	Material	H_2 and NO_2	…	…	12%
134	Graphene	Combination	NO_2	20 nA at 200 ppm	…	40%
119	Ag NWs/PPy functionalized graphene	Material	Dimethyl methylphosphonate (DMMP)	0.5% ppm^{-1}	5–25 ppm	20%
199	rGO/elastic yarn	Geometry	NO_2	55% at 5 ppm	0.5–10 ppm	400%
200	Crumpled PbS QD	Geometry	NO_2	3.7 ppm^{-1} from 0 to 20 ppm	1–150 ppm	90%
201	rGO and Ag NWs on PU sponge	Material	NO_2	…	5–100 ppm	60%
83	Multiwall nanotube (MWNT)/SnO_2 NW sensor with liquid metal interconnection	Combination	NO_2	1.2 at 200 ppm	…	50%
202	Woven PDMS-carbon fiber PPy	Combination	Various volatile organic compounds (VOCs)	…	Up to 1200 ppm	11%
203	Meniscus-guided MTs of PMMA/PPy	Geometry	NH_3	≈0.14 at 1 ppm ≈3.3 at 1000 ppm	1–1000 ppm	80%
204	rGO on mogul-patterned substrate	Geometry	NO_2	2.5% ppm^{-1} at 0% 2.3% ppm^{-1} at 30%	2.5–25 ppm	30%

depletion of carriers from the valence band and cause an increase in electrical resistance.

In 2016, Park *et al.* fabricated a transparent FET-based sensor [Fig. 8(c)] using Ag NWs and graphene hybrid nanostructures functionalized with drop-coated PPy for detecting dimethyl methylphosphonate (DMMP).[119] The transfer curves (V_G–I_D) and output curves (V_D–I_D) of the fabricated graphene FETs show a strong dependency on the surface conditions of the graphene channel [Fig. 8(d)]. For the triboelectric generator-based gas sensor, in 2017, Fu *et al.* fabricated a stretchable, carbon fiber-electronic skin (e-skin) [Fig. 8(e)] for detecting various volatile organic compounds (VOCs) based on the triboelectrification/gas-sensing coupling effect.[202] The triboelectric current of the e-skin was dependent on the concentration of methanol vapor [Fig. 8(f)].

Recently, 2D materials such as graphene, rGO, and MoS_2 have been considered as promising materials for gas sensing because their electronic properties are strongly affected by the adsorption of foreign molecules. For instance, graphene has been used as the gas sensor for NO_2, NH_3, and H_2,[205] due to its excellent properties, including high carrier mobility and 2D structures with a high exposed surface area. Because the intrinsic stretchability of these 2D materials is usually very limited, a geometry-engineering approach has been widely used in the community to achieve stretchable gas sensors. In 2016, Yun *et al.* reported a stretchable patterned graphene chemiresistor array in an island-bridge configuration.[134] The deformable soft Ecoflex substrate effectively suppressed the applied strain on the stiff SU-8 island supported chemiresistor and serpentine stretchable interconnections. In the same year, Lee *et al.* designed a mogul-patterned substrate with rGO being the sensitive material for stretchable gas sensors that can be stretched in multi-directions [Fig. 8(g)].[204] The applied stress in the layers on the mogul-patterned substrate can be efficiently absorbed, resulting in minimal interference with motion-induced stress. In a demonstration, an rGO chemiresistor fabricated on a mogul-patterned stretchable PDMS substrate exhibited no significant change in performance under stretching up to 30%. In 2017, Yan *et al.* reported a stretchable gas sensor through *in situ* preparation of PANI/MoS_2 nanocomposites onto the pre-strained PDMS substrate.[197] The assembled stretchable sensor demonstrated sensing performance as low as 50 ppb. In 2018, Yun *et al.* reported a stretchable chemiresistor composed of rGO sheets and highly elastic commercial yarns with high NO_2 sensitivity.[199] The rGO chemiresistor, which achieved its high stretchability based on a pre-strain strategy using commercial elastic yarns, showed a high NO_2 sensitivity of 55% at 5.0 ppm under 200% strain and outstanding mechanical stability (5000 cycles at 400% applied strain).

Other materials, including metal oxide[198] and conducting polymers,[197] have been used to produce stretchable chemiresistors. In 2017, Won *et al.* produced meniscus-guided freestanding microarchs of PMMA/PPy [Fig. 8(h)] using the colloidal solution of the composite polymer.[203] The stretchable PMMA/PPy gas sensors showed consistent sensitivities and responsiveness and recovery times up to 80% tensile strain for various NH_3 concentrations (possibly 1 to 1000 ppm). In 2016, Kim *et al.* reported an island-bridge configured stretchable gas-sensing system [Fig. 8(i)] with MWNT/SnO_2 NW being the sensing material.[83] The sensor was built on top of a stiff polyethylene terephthalate (PET) island and integrated on the Ecoflex substrate with Galinstan interconnections. Because of the much higher modulus of PET (2.0 to 2.7 GPa) compared to that of the Ecoflex (~69 kPa), the maximum principal strain of the PET island is only 0.05% even though the strain of the Ecoflex adjacent to the PET island is about 240%.

It should be noted that despite the recent progress toward producing stretchable gas sensors that can operate at room temperature, these devices usually have a poor response and recovery kinetics. Particularly, water molecules in the ambient air tend to adsorb on the surface of sensing materials and thus hinder the gas-solid interaction. Considering the solution processability of colloidal quantum dots, it has enabled the use of a wide variety of substrates and offers many degrees of freedom in sensor design. In 2018, Song *et al.* reported a fully stretchable, room-temperature-operable gas sensor with enhanced stability against humidity based on a crumpled PbS QD sensing layer placed on an elastomeric substrate with flexible graphene as electrodes.[200]

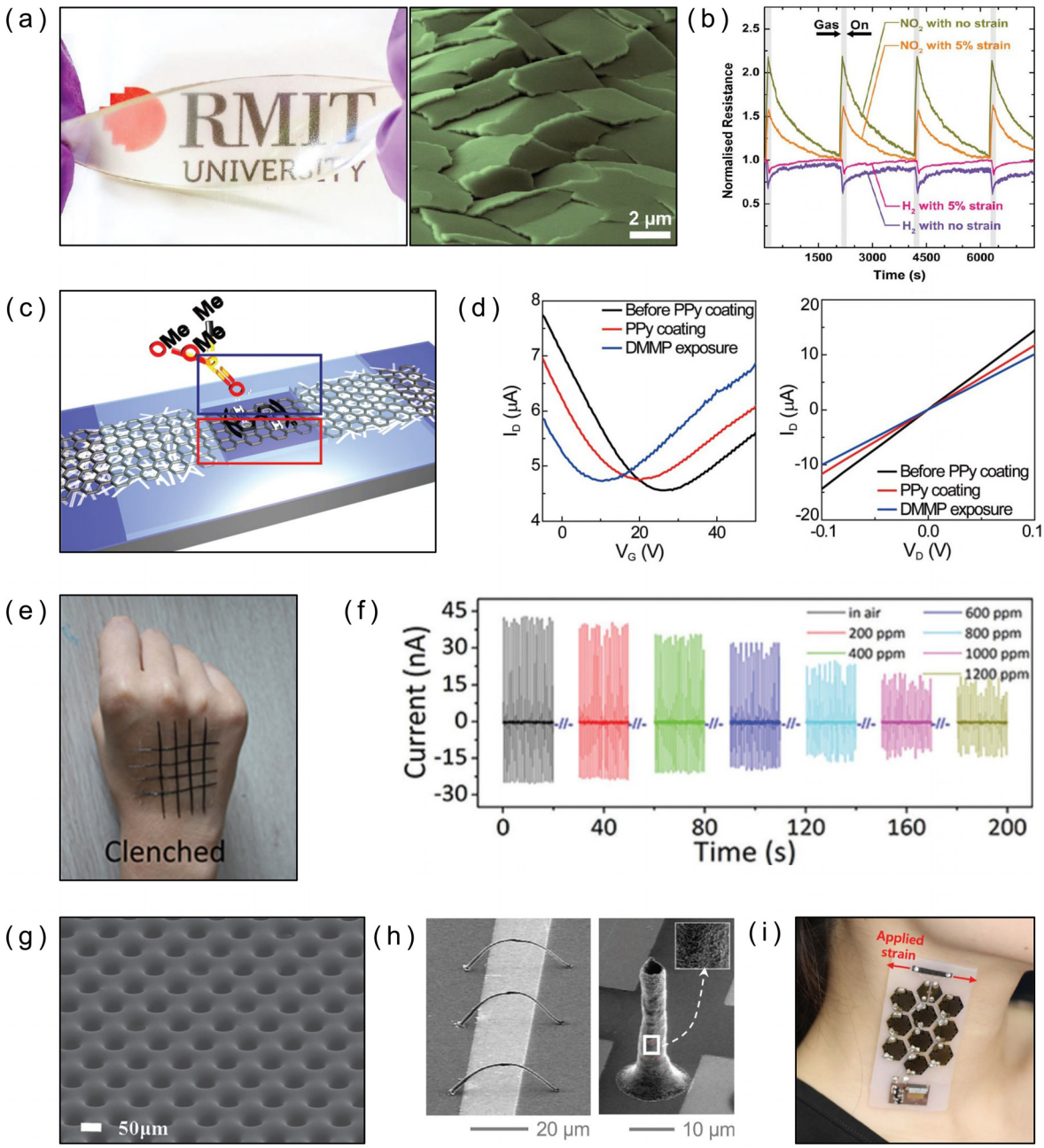

FIG. 8. Stretchable gas sensors. (a) Transparent and stretchable microtectonic ZnO gas sensor. The false-color SEM image shows the surface-cracked microtectonic surface of ZnO.[198] (b) Room temperature response of the microtectonic sensor to H_2 and NO_2 in relaxed and stretched states.[198] Reprinted with permission from P. Gutruf *et al.*, Small **11**, 4532 (2015). Copyright 2015 John Wiley and Sons. (c) Schematic illustrations of the FET-based graphene gas sensor for detecting DMMP.[119] (d) Transfer and output characteristics of graphene FET according to the coating conditions ($V_D = 0.05$ V or $V_G = 0$ V).[119] Reprinted with permission from J. Park *et al.*, Nanoscale **8**, 10591 (2016). Copyright 2016 Royal Society of Chemistry. (e) Carbon fiber-based electronic skin for gas sensing.[202] (f) The short-circuit current of the e-skin at different concentrations of methanol vapor with a constant deformation condition (601 bending, 1 Hz).[202] Reprinted with permission from Y. M. Fu *et al.*, J. Mater. Chem. C **5**, 1231 (2017). Copyright 2017 Royal Society of Chemistry. (g) Tilted-view SEM image of the PDMS substrate with the mogul pattern for a stretchable gas sensor.[204] Reprinted with permission from H. B. Lee *et al.*, Adv. Mater. **28**, 3069 (2016). Copyright 2016 John Wiley and Sons. (h) SEM images show the 3D microarch arrays (left) and the single microtube (right) with controlled dimensions and accurate individual positioning on the desired position.[203] Reprinted with permission from K. H. Won *et al.*, Curr. Appl. Phys. **17**, 339 (2017). Copyright 2016 Elsevier B.V. (i) Photograph of a stretchable multisensor array with the MWNT/SnO_2 NW hybrid gas sensing film in an island-bridge configuration.[83] Reprinted with permission from D. Kim *et al.*, Adv. Mater. **28**, 748 (2016). Copyright 2016 John Wiley and Sons.

IV. CONCLUSIONS AND CHALLENGES

The development of next-generation environmental sensors that can be integrated on or within the human body, animals, robots, industrial components, and natural assets will enable the IoT and will have positive environmental and economic implications. Such sensors will enable environmental issues such as air pollution, soil and water contamination, exposure to toxic substances, and noise pollution to be identified, monitored, and mitigated. This will significantly improve the health of humans, fish, and wildlife and promote sustainable development of natural ecosystems. In this review, we summarized the latest achievements in stretchable environmental sensors for monitoring light, temperature, humidity, pH, and gases. This novel class of environmental sensors allows sensors to be integrated into objects with curvilinear and movable 3D surfaces that are not possible otherwise for conventional electronics that are rigid and planar. By employing novel design concepts and device structures, two strategies have been pursued to achieve mechanical stretchability while maintaining electrical continuity: geometry engineering and material innovation. Geometry-engineered sensors achieve stretchability by optimizing the non-stretchable materials into novel in-plane (meander, serpentine, and horseshoe) and out-of-plane (wavy, buckled, and crumpled) geometries to absorb the applied strain. Innovative material-enabled stretchable sensors achieve the stretchability through synthesizing stretchable materials from a macroscopic viewpoint (intrinsically stretchable materials or nanocomposites), thereby enabling an intimate contact and integration to curvilinear surfaces and soft tissues. The combination of these two approaches, in some instances, has enabled further enhanced mechanical compliance and sensor performance.

However, remaining challenges concerning the stability and resilience of the stretchable devices over long-time and repeated mechanical stress must be overcome. Even though geometry-engineered stretchable sensors show consistent performance under different applied strains, they are mostly limited to a lower maximum stretchability. On the other hand, advances in understanding of nanomaterial phenomena and micro- and nanofabrication technologies have enabled intrinsically stretchable materials that are much softer and more stretchable to intimately integrate on soft tissues. However, they usually suffer from degraded performance when the tensile strain is increased. Moreover, it should be noted that currently available results about stretchable sensors are usually obtained in idealized laboratory environments with controlled environmental stimulus. When bringing these devices from the laboratory to the real-world environment with a wide-range of fluctuating parameters such as temperature, humidity, and gas compositions, these devices should be evaluated fully to establish their stabilities.

Next-generation stretchable environmental sensors are envisioned to be the core part of IoT. The ability to sense multiple environmental stimuli in a single device is an ultimate goal for environmental sensors and is of critical importance in developing smart and interactive stretchable sensors. However, currently available environmental sensors have mainly focused on single or dual sensory functionalities. A simultaneous detection and high selectivity of multi-complex stimuli from the ambient environment remains a challenge. As discussed in this article, most of the stretchable environmental sensors are responsive to multiple stimuli, such as temperature, humidity, and the mechanical disturbances. For instance, GO is shown to be dependent on both temperature and humidity. Extraction of humidity would require prior knowledge of temperature. Deduction from the obtained measurements to the desired physical/chemical quantities is not always straightforward. Selectivity of the device should be carefully evaluated against all the possible environmental parameters and the relationship to the applied strain to the device. Incorporating commercial off-the-shelf sensors with stretchable substrates in an island-bridge geometry and integrating the stretchable sensors into multiple layers[206,207] provide one of the paths to solve this challenge.

In terms of the use of nanomaterials in these devices, the cost needs to be lowered and their environmental effect should be carefully evaluated. Several studies have also revealed that engineered nanomaterials, depending on their size, shape, surface area, chemical composition, and biopersistence, may have possible health impacts on the environment and humans.[208–210] These materials need to be carefully assessed before entering the market and being exposed to the environment.

ACKNOWLEDGMENTS

This study was funded by the U.S. Department of Energy Water Power Technologies Office and was conducted at the Pacific Northwest National Laboratory, which is operated by Battelle for the Department of Energy under Contract No. DE-AC05-76RL01830. Y.Y. acknowledges Artwork (Figure 1) from Xiao-Meng Wu.

REFERENCES

[1]S. U. Goldenberg, I. Nagelkerken, E. Marangon, A. Bonnet, C. M. Ferreira, and S. D. Connell, Nat. Clim. Change **8**, 229 (2018).
[2]J. Ma and J. Xu, Nature **541**, 30 (2017).
[3]B. Petrie, R. Barden, and B. Kasprzyk-Hordern, Water Res. **72**, 3 (2015).
[4]M. Kampa and E. Castanas, Environ. Pollut. **151**, 362 (2008).
[5]M. Gavrilescu, K. Demnerova, J. Aamand, S. Agathos, and F. Fava, New Biotechnol. **32**, 147 (2015).
[6]See https://www.worldbank.org/en/topic/environment/overview for Environment At-A-Glance.
[7]See http://www.who.int/gho/publications/en/ for Global Health Observatory (GHO) data for Global Health Observatory (GHO) data.
[8]R. Lucas, T. McMichael, W. Smith, B. K. Armstrong, and A. Prüss-Üstün, *Solar Ultraviolet Radiation: Global Burden of Disease from Solar Ultraviolet Radiation* (World Health Organization, 2006).
[9]R. P. Schwarzenbach, B. I. Escher, K. Fenner, T. B. Hofstetter, C. A. Johnson, U. von Gunten, and B. Wehrli, Science **313**, 1072 (2006).
[10]G. Woodward, M. O. Gessner, P. S. Giller, V. Gulis, S. Hladyz, A. Lecerf, B. Malmqvist, B. G. McKie, S. D. Tiegs, H. Cariss, M. Dobson, A. Elosegi, V. Ferreira, M. A. Graca, T. Fleituch, J. O. Lacoursiere, M. Nistorescu, J. Pozo, G. Risnoveanu, M. Schindler, A. Vadineanu, L. B. Vought, and E. Chauvet, Science **336**, 1438 (2012).
[11]Z. Q. Deng, T. J. Carlson, D. D. Dauble, and G. R. Ploskey, Energies **4**, 57 (2011).
[12]Z. H. Zhou, X. S. Li, Y. F. Wu, H. Zhang, Z. W. Lin, K. Y. Meng, Z. M. Lin, Q. He, C. C. Sun, J. Yang, and Z. L. Wang, Nano Energy **53**, 501 (2018).
[13]C. K. Ho, A. Robinson, D. R. Miller, and M. J. Davis, Sensors **5**, 4 (2005).

[14]R. W. Keyes, Proc. IEEE **89**, 227 (2001).
[15]See https://waterpower.pnnl.gov/jsats/ for Injectable Acoustic Tag.
[16]D.-H. Kim, N. Lu, R. Ma, Y.-S. Kim, R.-H. Kim, S. Wang, J. Wu, S. M. Won, H. Tao, and A. Islam, Science **333**, 838 (2011).
[17]Y. Yang, T. Vervust, S. Dunphy, S. Van Put, B. Vandecasteele, K. Dhaenens, L. Degrendele, L. Mader, L. D. Vriese, and T. Martens, Adv. Electron. Mater. **4**(8), 1800071 (2018).
[18]S. Wang, J. Xu, W. Wang, G. N. Wang, R. Rastak, F. Molina-Lopez, J. W. Chung, S. Niu, V. R. Feig, J. Lopez, T. Lei, S. K. Kwon, Y. Kim, A. M. Foudeh, A. Ehrlich, A. Gasperini, Y. Yun, B. Murmann, J. B. Tok, and Z. Bao, Nature **555**, 83 (2018).
[19]M. Kaltenbrunner, T. Sekitani, J. Reeder, T. Yokota, K. Kuribara, T. Tokuhara, M. Drack, R. Schwodiauer, I. Graz, S. Bauer-Gogonea, S. Bauer, and T. Someya, Nature **499**, 458 (2013).
[20]T. Yamada, Y. Hayamizu, Y. Yamamoto, Y. Yomogida, A. Izadi-Najafabadi, D. N. Futaba, and K. Hata, Nat. Nanotechnol. **6**, 296 (2011).
[21]M. C. Zhang, C. Y. Wang, X. P. Liang, Z. Yin, K. L. Xia, H. Wang, M. Q. Jian, and Y. Y. Zhang, Adv. Electron. Mater. **3**, 1700193 (2017).
[22]X. Fan, B. G. Xu, N. X. Wang, J. Z. Wang, S. H. Liu, H. Wang, and F. Yan, Adv. Electron. Mater. **3**, 1600471 (2017).
[23]S. Rosset and H. R. Shea, Appl. Phys. Rev. **3**, 031105 (2016).
[24]Y. C. Lai, B. W. Ye, C. F. Lu, C. T. Chen, M. H. Jao, W. F. Su, W. Y. Hung, T. Y. Lin, and Y. F. Chen, Adv. Funct. Mater. **26**, 1286 (2016).
[25]X. Ji, A. El Haitami, F. Sorba, S. Rosset, G. T. Nguyen, C. Plesse, F. Vidal, H. R. Shea, and S. Cantin, Sens. Actuator, B **261**, 135 (2018).
[26]S. Xu, Y. Zhang, J. Cho, J. Lee, X. Huang, L. Jia, J. A. Fan, Y. Su, J. Su, H. Zhang, H. Cheng, B. Lu, C. Yu, C. Chuang, T. I. Kim, T. Song, K. Shigeta, S. Kang, C. Dagdeviren, I. Petrov, P. V. Braun, Y. Huang, U. Paik, and J. A. Rogers, Nat. Commun. **4**, 1543 (2013).
[27]D. J. Lipomi, B. C. Tee, M. Vosgueritchian, and Z. Bao, Adv. Mater. **23**, 1771 (2011).
[28]L. Hu, M. Pasta, F. L. Mantia, L. Cui, S. Jeong, H. D. Deshazer, J. W. Choi, S. M. Han, and Y. Cui, Nano Lett. **10**, 708 (2010).
[29]T. Sekitani, Y. Noguchi, K. Hata, T. Fukushima, T. Aida, and T. Someya, Science **321**, 1468 (2008).
[30]T. Sekitani, H. Nakajima, H. Maeda, T. Fukushima, T. Aida, K. Hata, and T. Someya, Nat. Mater. **8**, 494 (2009).
[31]J. J. Liang, L. Li, X. F. Niu, Z. B. Yu, and Q. B. Pei, Nat. Photonics **7**, 817 (2013).
[32]S. Russo, T. Ranzani, H. Liu, S. Nefti-Meziani, K. Althoefer, and A. Menciassi, Soft Rob. **2**, 146 (2015).
[33]D. Kai, S. Jiang, Z. W. Low, and X. J. Loh, J. Mater. Chem. B **3**, 6194 (2015).
[34]Y. C. Lai, J. Deng, S. L. Zhang, S. Niu, H. Guo, and Z. L. Wang, Adv. Funct. Mater. **27**, 1604462 (2017).
[35]Y. C. Lai, J. Deng, R. Liu, Y. C. Hsiao, S. L. Zhang, W. Peng, H. M. Wu, X. Wang, and Z. L. Wang, Adv. Mater. **30**(28), 1801114 (2018).
[36]K. Takei, *Flexible and Stretchable Medical Devices* (John Wiley & Sons, 2018).
[37]J. A. Rogers, T. Someya, and Y. Huang, Science **327**, 1603 (2010).
[38]J. Vanfleteren, M. Gonzalez, F. Bossuyt, Y. Y. Hsu, T. Vervust, I. De Wolf, and M. Jablonski, MRS Bull. **37**, 254 (2012).
[39]T. Vervust, G. Buyle, F. Bossuyt, and J. Vanfleteren, J. Textile Inst. **103**, 1127 (2012).
[40]I. M. Graz and S. P. Lacour, Org. Electron. **11**, 1815 (2010).
[41]C. H. Yang and Z. G. Suo, Nat. Rev. Mater. **3**, 125 (2018).
[42]H. Wang, Z. Wang, J. Yang, C. Xu, Q. Zhang, and Z. Peng, Macromol. Rapid Commun. **39**, e1800246 (2018).
[43]Z. Ma, B. Su, S. Gong, Y. Wang, L. W. Yap, G. P. Simon, and W. L. Cheng, ACS Sens. **1**, 303 (2016).
[44]D. J. Lipomi, J. A. Lee, M. Vosgueritchian, B. C. K. Tee, J. A. Bolander, and Z. A. Bao, Chem. Mater. **24**, 373 (2012).
[45]J. Xu, S. Wang, G.-J. N. Wang, C. Zhu, S. Luo, L. Jin, X. Gu, S. Chen, V. R. Feig, and J. W. To, Science **355**, 59 (2017).
[46]K. Suzuki, K. Yataka, Y. Okumiya, S. Sakakibara, K. Sako, H. Mimura, and Y. Inoue, ACS Sens. **1**, 817 (2016).
[47]P. Lee, J. Lee, H. Lee, J. Yeo, S. Hong, K. H. Nam, D. Lee, S. S. Lee, and S. H. Ko, Adv. Mater. **24**, 3326 (2012).
[48]H. W. Cui, K. Suganuma, and H. Uchida, Nano Res. **8**, 1604 (2015).
[49]Y. Yang, S. Ding, T. Araki, J. Jiu, T. Sugahara, J. Wang, J. Vanfleteren, T. Sekitani, and K. Suganuma, Nano Res. **9**, 401 (2016).
[50]F. Xu, W. Lu, and Y. Zhu, ACS Nano **5**, 672 (2011).
[51]S. Gong and W. Cheng, Adv. Electron. Mater. **3**, 1600314 (2017).
[52]J. Kim, R. Kumar, A. J. Bandodkar, and J. Wang, Adv. Electron. Mater. **3**, 1600260 (2017).
[53]W. Liu, M. S. Song, B. Kong, and Y. Cui, Adv. Mater. **29**, 1603436 (2017).
[54]T. T. Yang, D. Xie, Z. H. Li, and H. W. Zhu, Mater. Sci. Eng. R **115**, 1 (2017).
[55]J. H. Koo, D. C. Kim, H. J. Shim, T. H. Kim, and D. H. Kim, Adv. Funct. Mater. **28**, 1801834 (2018).
[56]S. Yao, P. Swetha, and Y. Zhu, Adv. Healthcare Mater. **7**, 1700889 (2018).
[57]Y. Liu, M. Pharr, and G. A. Salvatore, ACS Nano **11**, 9614 (2017).
[58]D. Y. Khang, H. Jiang, Y. Huang, and J. A. Rogers, Science **311**, 208 (2006).
[59]W. M. Choi, J. Song, D.-Y. Khang, H. Jiang, Y. Y. Huang, and J. A. Rogers, Nano Lett. **7**, 1655 (2007).
[60]Y. Sun, W. M. Choi, H. Jiang, Y. Y. Huang, and J. A. Rogers, Nat. Nanotechnol. **1**, 201 (2006).
[61]K. I. Jang, K. Li, H. U. Chung, S. Xu, H. N. Jung, Y. Yang, J. W. Kwak, H. H. Jung, J. Song, C. Yang, A. Wang, Z. Liu, J. Y. Lee, B. H. Kim, J. H. Kim, J. Lee, Y. Yu, B. J. Kim, H. Jang, K. J. Yu, J. Kim, J. W. Lee, J. W. Jeong, Y. M. Song, Y. Huang, Y. Zhang, and J. A. Rogers, Nat. Commun. **8**, 15894 (2017).
[62]M. Gonzalez, F. Axisa, M. V. BuIcke, D. Brosteaux, B. Vandevelde, and J. Vanfleteren, Microelectron. Reliab. **48**, 825 (2008).
[63]J. van den Brand, M. De Kok, M. Koetse, M. Cauwe, R. Verplancke, F. Bossuyt, M. Jablonski, and J. Vanfleteren, Solid State Electron. **113**, 116 (2015).
[64]J. Zang, S. Ryu, N. Pugno, Q. Wang, Q. Tu, M. J. Buehler, and X. Zhao, Nat. Mater. **12**, 321 (2013).
[65]S. H. Chae, W. J. Yu, J. J. Bae, D. L. Duong, D. Perello, H. Y. Jeong, Q. H. Ta, T. H. Ly, Q. A. Vu, and M. Yun, Nat. Mater. **12**, 403 (2013).
[66]T. Chen, Y. Xue, A. K. Roy, and L. Dai, ACS Nano **8**, 1039 (2014).
[67]S. G. Lee, H. Kim, H. H. Choi, H. Bong, Y. D. Park, W. H. Lee, and K. Cho, Adv. Mater. **25**, 2162 (2013).
[68]H. Ryu, S. J. Cho, B. Kim, and G. Lim, RSC Adv. **4**, 39767 (2014).
[69]S. Xu, Z. Yan, K. I. Jang, W. Huang, H. Fu, J. Kim, Z. Wei, M. Flavin, J. McCracken, R. Wang, A. Badea, Y. Liu, D. Xiao, G. Zhou, J. Lee, H. U. Chung, H. Cheng, W. Ren, A. Banks, X. Li, U. Paik, R. G. Nuzzo, Y. Huang, Y. Zhang, and J. A. Rogers, Science **347**, 154 (2015).
[70]D. Brosteaux, F. Axisa, M. Gonzalez, and J. Vanfleteren, IEEE Electron Device Lett. **28**, 552 (2007).
[71]Y. Y. Hsu, M. Gonzalez, F. Bossuyt, J. Vanfleteren, and I. De Wolf, IEEE Trans. Electron Devices **58**, 2680 (2011).
[72]Y. Y. Hsu, M. Gonzalez, F. Bossuyt, F. Axisa, J. Vanfleteren, and I. De Wolf, Thin Solid Films **519**, 2225 (2011).
[73]J. A. Fan, W. H. Yeo, Y. Su, Y. Hattori, W. Lee, S. Y. Jung, Y. Zhang, Z. Liu, H. Cheng, L. Falgout, M. Bajema, T. Coleman, D. Gregoire, R. J. Larsen, Y. Huang, and J. A. Rogers, Nat. Commun. **5**, 3266 (2014).
[74]Y. H. Zhang, S. D. Wang, X. T. Li, J. A. Fan, S. Xu, Y. M. Song, K. J. Choi, W. H. Yeo, W. Lee, S. N. Nazaar, B. W. Lu, L. Yin, K. C. Hwang, J. A. Rogers, and Y. G. Huang, Adv. Funct. Mater. **24**, 2028 (2014).
[75]S. Xu, Y. Zhang, L. Jia, K. E. Mathewson, K. I. Jang, J. Kim, H. Fu, X. Huang, P. Chava, R. Wang, S. Bhole, L. Wang, Y. J. Na, Y. Guan, M. Flavin, Z. Han, Y. Huang, and J. A. Rogers, Science **344**, 70 (2014).
[76]F. Bossuyt, T. Vervust, and J. Vanfleteren, IEEE Trans. Compon., Packag., Manuf. Technol. **3**, 229 (2013).
[77]Y. Yang, G. Chiesura, B. Plovie, T. Vervust, G. Luyckx, J. Degrieck, T. Sekitani, and J. Vanfleteren, ACS Sens. **3**, 1698 (2018).
[78]Y. Yang, K. Xu, T. Vervust, and J. Vanfleteren, Sens. Actuator B **261**, 144 (2018).
[79]H. C. Ko, M. P. Stoykovich, J. Song, V. Malyarchuk, W. M. Choi, C. J. Yu, J. B. Geddes 3rd, J. Xiao, S. Wang, Y. Huang, and J. A. Rogers, Nature **454**, 748 (2008).
[80]S. Y. Hong, Y. H. Lee, H. Park, S. W. Jin, Y. R. Jeong, J. Yun, I. You, G. Zi, and J. S. Ha, Adv. Mater. **28**, 930 (2016).
[81]J. Kim, M. Lee, H. J. Shim, R. Ghaffari, H. R. Cho, D. Son, Y. H. Jung, M. Soh, C. Choi, S. Jung, K. Chu, D. Jeon, S. T. Lee, J. H. Kim, S. H. Choi, T. Hyeon, and D. H. Kim, Nat. Commun. **5**, 5747 (2014).

[82]S. W. Hwang, C. H. Lee, H. Cheng, J. W. Jeong, S. K. Kang, J. H. Kim, J. Shin, J. Yang, Z. Liu, G. A. Ameer, Y. Huang, and J. A. Rogers, Nano Lett. **15**, 2801 (2015).
[83]D. Kim, D. Kim, H. Lee, Y. R. Jeong, S. J. Lee, G. Yang, H. Kim, G. Lee, S. Jeon, and G. Zi, Adv. Mater. **28**, 748 (2016).
[84]J. Vanfleteren, I. Chtioui, B. Plovie, Y. Yang, F. Bossuyt, T. Vervust, S. Dunphy, and B. Vandecasteele, Proc. Technol. **15**, 208 (2014).
[85]B. Plovie, Y. Yang, J. Guillaume, S. Dunphy, K. Dhaenens, S. Van Put, B. Vandecasteele, T. Vervust, F. Bossuyt, and J. Vanfleteren, Adv. Eng. Mater. **19**, 1700032 (2017).
[86]Y. Yang, G. Chiesura, T. Vervust, F. Bossuyt, G. Luyckx, M. Kaufmann, J. Degrieck, and J. Vanfleteren, MRS Online Proc. Libr. Arch. **1798**, 2136585 (2015).
[87]S. Biswas, A. Schoberl, M. Mozafari, J. Pezoldt, T. Stauden, and H. O. Jacobs, NPG Asia Mater. **8**, e336 (2016).
[88]M. D. Dickey, Adv. Mater. **29**, 1606425 (2017).
[89]M. D. Dickey, R. C. Chiechi, R. J. Larsen, E. A. Weiss, D. A. Weitz, and G. M. Whitesides, Adv. Funct. Mater. **18**, 1097 (2008).
[90]R. K. Kramer, C. Majidi, and R. J. Wood, Adv. Funct. Mater. **23**, 5292 (2013).
[91]H. Ota, S. Emaminejad, Y. J. Gao, A. Zhao, E. Wu, S. Challa, K. Chen, H. M. Fahad, A. K. Jha, D. Kiriya, W. Gao, H. Shiraki, K. Morioka, A. R. Ferguson, K. E. Healy, R. W. Davis, and A. Javey, Adv. Mater. Technol. **1**, 1600013 (2016).
[92]H. Ota, K. Chen, Y. Lin, D. Kiriya, H. Shiraki, Z. Yu, T. J. Ha, and A. Javey, Nat. Commun. **5**, 5032 (2014).
[93]F. Xu and Y. Zhu, Adv. Mater. **24**, 5117 (2012).
[94]H. Wu, D. Kong, Z. Ruan, P. C. Hsu, S. Wang, Z. Yu, T. J. Carney, L. Hu, S. Fan, and Y. Cui, Nat. Nanotechnol. **8**, 421 (2013).
[95]Y. L. Liu, Y. Qin, Z. H. Jin, X. B. Hu, M. M. Chen, R. Liu, C. Amatore, and W. H. Huang, Angew. Chem. Int. Ed. **56**, 9454 (2017).
[96]Y. Kim, J. Zhu, B. Yeom, M. Di Prima, X. Su, J. G. Kim, S. J. Yoo, C. Uher, and N. A. Kotov, Nature **500**, 59 (2013).
[97]Y. G. Hu, T. Zhao, P. L. Zhu, Y. Zhang, X. W. Liang, R. Sun, and C. P. Wong, Nano Res. **11**, 1938 (2018).
[98]N. Matsuhisa, D. Inoue, P. Zalar, H. Jin, Y. Matsuba, A. Itoh, T. Yokota, D. Hashizume, and T. Someya, Nat. Mater. **16**, 834 (2017).
[99]C.-F. Li, W. Li, H. Zhang, J. Jiu, Y. Yang, L. Li, Y. Gao, Z.-Q. Liu, and K. Suganuma, ACS Appl. Mater. Interfaces **11**, 3231 (2018).
[100]M. Park, J. Im, M. Shin, Y. Min, J. Park, H. Cho, S. Park, M. B. Shim, S. Jeon, D. Y. Chung, J. Bae, J. Park, U. Jeong, and K. Kim, Nat. Nanotechnol. **7**, 803 (2012).
[101]K. Y. Chun, Y. Oh, J. Rho, J. H. Ahn, Y. J. Kim, H. R. Choi, and S. Baik, Nat. Nanotechnol. **5**, 853 (2010).
[102]D. C. Hyun, M. Park, C. Park, B. Kim, Y. Xia, J. H. Hur, J. M. Kim, J. J. Park, and U. Jeong, Adv. Mater. **23**, 2946 (2011).
[103]R. K. Mishra, L. J. Hubble, A. Martin, R. Kumar, A. Barfidokht, J. Kim, M. M. Musameh, I. L. Kyratzis, and J. Wang, ACS Sens. **2**, 553 (2017).
[104]S. Iijima, Nature **354**, 56 (1991).
[105]J. W. Wilder, L. C. Venema, A. G. Rinzler, R. E. Smalley, and C. Dekker, Nature **391**, 59 (1998).
[106]F. Li, H. M. Cheng, S. Bai, G. Su, and M. S. Dresselhaus, Appl. Phys. Lett. **77**, 3161 (2000).
[107]B. G. Demczyk, Y. M. Wang, J. Cumings, M. Hetman, W. Han, A. Zettl, and R. O. Ritchie, Mater. Sci. Eng. A **334**, 173 (2002).
[108]J. P. Salvetat, A. J. Kulik, J. M. Bonard, G. A. D. Briggs, T. Stockli, K. Metenier, S. Bonnamy, F. Beguin, N. A. Burnham, and L. Forro, Adv. Mater. **11**, 161 (1999).
[109]H. Dai, Acc. Chem. Res. **35**, 1035 (2002).
[110]C. Chen, J. Cao, X. Y. Wang, Q. Q. Lu, M. M. Han, Q. R. Wang, H. T. Dai, Z. Q. Niu, J. Chen, and S. S. Xie, Nano Energy **42**, 187 (2017).
[111]H. Yang, D. Qi, Z. Liu, B. K. Chandran, T. Wang, J. Yu, and X. Chen, Adv. Mater. **28**, 9175 (2016).
[112]S. Y. Oh, S. Y. Hong, Y. R. Jeong, J. Yun, H. Park, S. W. Jin, G. Lee, J. H. Oh, H. Lee, S. S. Lee, and J. S. Ha, ACS Appl. Mater. Interfaces **10**, 13729 (2018).
[113]S. Y. Kim, S. Park, H. W. Park, D. H. Park, Y. Jeong, and D. H. Kim, Adv. Mater. **27**, 4178 (2015).
[114]G. Zhou, J. H. Byun, Y. Oh, B. M. Jung, H. J. Cha, D. G. Seong, M. K. Um, S. Hyun, and T. W. Chou, ACS Appl. Mater. Interfaces **9**, 4788 (2017).
[115]S. Gong, W. Schwalb, Y. Wang, Y. Chen, Y. Tang, J. Si, B. Shirinzadeh, and W. Cheng, Nat. Commun. **5**, 3132 (2014).
[116]R. R. Wang, H. T. Zhai, T. Wang, X. Wang, Y. Cheng, L. J. Shi, and J. Sun, Nano Res. **9**, 2138 (2016).
[117]S. Ding, J. Jiu, Y. Gao, Y. Tian, T. Araki, T. Sugahara, S. Nagao, M. Nogi, H. Koga, K. Suganuma, and H. Uchida, ACS Appl. Mater. Interfaces **8**, 6190 (2016).
[118]J. Jiu, T. Araki, J. Wang, M. Nogi, T. Sugahara, S. Nagao, H. Koga, K. Suganuma, E. Nakazawa, M. Hara, H. Uchida, and K. Shinozaki, J. Mater. Chem. A **2**, 6326 (2014).
[119]J. Park, J. Kim, K. Kim, S. Y. Kim, W. H. Cheong, K. Park, J. H. Song, G. Namgoong, J. J. Kim, J. Heo, F. Bien, and J. U. Park, Nanoscale **8**, 10591 (2016).
[120]S. Han, M. K. Kim, B. Wang, D. S. Wie, S. Wang, and C. H. Lee, Adv. Mater. **28**, 10257 (2016).
[121]X. Xuan, J. Y. Kim, X. Hui, P. S. Das, H. S. Yoon, and J. Y. Park, Biosens. Bioelectron. **120**, 160 (2018).
[122]C. Keplinger, J. Y. Sun, C. C. Foo, P. Rothemund, G. M. Whitesides, and Z. Suo, Science **341**, 984 (2013).
[123]L. Hu, H. S. Kim, J.-Y. Lee, P. Peumans, and Y. Cui, ACS Nano **4**, 2955 (2010).
[124]J. Jiu, M. Nogi, T. Sugahara, T. Tokuno, T. Araki, N. Komoda, K. Suganuma, H. Uchida, and K. Shinozaki, J. Mater. Chem. **22**, 23561 (2012).
[125]E. C. Garnett, W. Cai, J. J. Cha, F. Mahmood, S. T. Connor, M. G. Christoforo, Y. Cui, M. D. McGehee, and M. L. Brongersma, Nat. Mater. **11**, 241 (2012).
[126]J. A. Schuller, E. S. Barnard, W. Cai, Y. C. Jun, J. S. White, and M. L. Brongersma, Nat. Mater. **9**, 193 (2010).
[127]C. Mayousse, C. Celle, A. Fraczkiewicz, and J.-P. Simonato, Nanoscale **7**, 2107 (2015).
[128]L. Y. Li, W. L. Li, J. T. Jiu, and K. Suganuma, Appl. Surf. Sci. **459**, 732 (2018).
[129]K. S. Kim, Y. Zhao, H. Jang, S. Y. Lee, J. M. Kim, K. S. Kim, J. H. Ahn, P. Kim, J. Y. Choi, and B. H. Hong, Nature **457**, 706 (2009).
[130]J. M. Gong, T. Zhou, D. D. Song, and L. Z. Zhang, Sens. Actuator B **150**, 491 (2010).
[131]X. Fu, T. Lou, Z. Chen, M. Lin, W. Feng, and L. Chen, ACS Appl. Mater. Interfaces **4**, 1080 (2012).
[132]J. Li, S. Guo, Y. Zhai, and E. Wang, Anal. Chim. Acta **649**, 196 (2009).
[133]A. Kundu, R. K. Layek, A. Kuila, and A. K. Nandi, ACS Appl. Mater. Interfaces **4**, 5576 (2012).
[134]J. Yun, Y. Lim, G. N. Jang, D. Kim, S. J. Lee, H. Park, S. Y. Hong, G. Lee, G. Zi, and J. S. Ha, Nano Energy **19**, 401 (2016).
[135]P. Kang, M. C. Wang, P. M. Knapp, and S. Nam, Adv. Mater. **28**, 4639 (2016).
[136]M. Kim, P. Kang, J. Leem, and S. Nam, Nanoscale **9**, 4058 (2017).
[137]M. Kataria, K. Yadav, G. Haider, Y. M. Liao, Y. R. Liou, S. Y. Cai, H. I. Lin, Y. H. Chen, C. R. P. Inbaraj, K. P. Bera, H. M. Lee, Y. T. Chen, W. H. Wang, and Y. F. Chen, ACS Photonics **5**, 2336 (2018).
[138]J. Ding, H. Fang, Z. Lian, Q. Lv, J.-L. Sun, and Q. Yan, Nanoscale **10**, 10538 (2018).
[139]S. Stankovich, D. A. Dikin, R. D. Piner, K. A. Kohlhaas, A. Kleinhammes, Y. Jia, Y. Wu, S. T. Nguyen, and R. S. Ruoff, Carbon **45**, 1558 (2007).
[140]X. Wang, I. Kholmanov, H. Chou, and R. S. Ruoff, ACS Nano **9**, 8737 (2015).
[141]M. J. McAllister, J.-L. Li, D. H. Adamson, H. C. Schniepp, A. A. Abdala, J. Liu, M. Herrera-Alonso, D. L. Milius, R. Car, and R. K. Prud'homme, Chem. Mater. **19**, 4396 (2007).
[142]C. R. Taylor, R. S. Stern, J. J. Leyden, and B. A. Gilchrest, J. Am. Acad. Dermatol. **22**, 1 (1990).
[143]M. Boulton, M. Rozanowska, and B. Rozanowski, J. Photochem. Photobiol., B **64**, 144 (2001).
[144]J. Barber and B. Andersson, Trends Biochem. Sci. **17**, 61 (1992).
[145]A. Melis, Trends Plant Sci. **4**, 130 (1999).
[146]T. Longcore and C. Rich, Front. Ecol. Environ. **2**, 191 (2004).
[147]J. Wang, C. Yan, W. Kang, and P. S. Lee, Nanoscale **6**, 10734 (2014).
[148]C. Yan, J. Wang, X. Wang, W. Kang, M. Cui, C. Y. Foo, and P. S. Lee, Adv. Mater. **26**, 943 (2014).

[149]S. Huang, C. F. Guo, X. Zhang, W. Pan, X. Luo, C. S. Zhao, J. H. Gong, X. Y. Li, Z. F. Ren, and H. Wu, Small **11**, 5712 (2015).
[150]J. Yoo, S. Jeong, S. Kim, and J. H. Je, Adv. Mater. **27**, 1712 (2015).
[151]T. Q. Trung, V. Q. Dang, H.-B. Lee, D.-I. Kim, S. Moon, N.-E. Lee, and H. Lee, ACS Appl. Mater. Interfaces **9**, 35958 (2017).
[152]Q. L. Guo, Y. F. Fang, M. Zhang, G. S. Huang, P. K. Chu, Y. F. Mei, Z. F. Di, and X. Wang, IEEE Trans. Electron Devices **64**, 1985 (2017).
[153]B. Sun, Y. Sun, and C. Wang, Small **14**, 1703391 (2018).
[154]Y. M. Song, Y. Xie, V. Malyarchuk, J. Xiao, I. Jung, K. J. Choi, Z. Liu, H. Park, C. Lu, R. H. Kim, R. Li, K. B. Crozier, Y. Huang, and J. A. Rogers, Nature **497**, 95 (2013).
[155]D. Kim, G. Shin, J. Yoon, D. Jang, S. J. Lee, G. Zi, and J. S. Ha, Nanotechnology **24**, 315502 (2013).
[156]G. Konstantatos and E. H. Sargent, Nat. Nanotechnol. **5**, 391 (2010).
[157]M. Liu and H. K. Kim, Appl. Phys. Lett. **84**, 173 (2004).
[158]J. T. Kim, S. K. Seol, J. Pyo, J. S. Lee, J. H. Je, and G. Margaritondo, Adv. Mater. **23**, 1968 (2011).
[159]J. T. Kim, J. Pyo, J. Rho, J. H. Ahn, J. H. Je, and G. Margaritondo, ACS Macro Lett. **1**, 375 (2012).
[160]X. Gan, R.-J. Shiue, Y. Gao, I. Meric, T. F. Heinz, K. Shepard, J. Hone, S. Assefa, and D. Englund, Nat. Photonics **7**, 883 (2013).
[161]G.-R. Walther, E. Post, P. Convey, A. Menzel, C. Parmesan, T. J. Beebee, J.-M. Fromentin, O. Hoegh-Guldberg, and F. Bairlein, Nature **416**, 389 (2002).
[162]T. Yokota, Y. Inoue, Y. Terakawa, J. Reeder, M. Kaltenbrunner, T. Ware, K. Yang, K. Mabuchi, T. Murakawa, M. Sekino, W. Voit, T. Sekitani, and T. Someya, Proc. Natl. Acad. Sci. U. S. A. **112**, 14533 (2015).
[163]J. Fraden, *Handbook of modern sensors: physics, designs, and applications* (Springer Science & Business Media, 2004).
[164]X. Liao, Q. Liao, Z. Zhang, X. Yan, Q. Liang, Q. Wang, M. Li, and Y. Zhang, Adv. Funct. Mater. **26**, 3074 (2016).
[165]C. Yingzhi, X. Yin, K. Yujie, L. Wenhao, L. Yi, L. Jingyuan, W. Lu-Ning, and Z. Xiaohong, Sci. China Mater. **61**, 969 (2018).
[166]C. J. Yu, Z. Y. Wang, H. Y. Yu, and H. Q. Jiang, Appl. Phys. Lett. **95**, 141912 (2009).
[167]Y. Chen, B. Lu, Y. Chen, and X. Feng, Sci. Rep. **5**, 11505 (2015).
[168]C. Yan, J. Wang, and P. S. Lee, ACS Nano **9**, 2130 (2015).
[169]Y. He, Q. Gui, S. Liao, H. Jia, and Y. Wang, Adv. Mater. Technol. **1**, 1600170 (2016).
[170]J. Yang, D. P. Wei, L. L. Tang, X. F. Song, W. Luo, J. Chu, T. P. Gao, H. F. Shi, and C. L. Du, RSC Adv. **5**, 25609 (2015).
[171]T. Q. Trung, S. Ramasundaram, B. U. Hwang, and N. E. Lee, Adv. Mater. **28**, 502 (2016).
[172]J. Wu, S. Han, T. Yang, Z. Li, Z. Wu, X. Gui, K. Tao, J. Miao, L. K. Norford, C. Liu, and F. Huo, ACS Appl. Mater. Interfaces **10**, 19097 (2018).
[173]R. C. Webb, A. P. Bonifas, A. Behnaz, Y. Zhang, K. J. Yu, H. Cheng, M. Shi, Z. Bian, Z. Liu, Y. S. Kim, W. H. Yeo, J. S. Park, J. Song, Y. Li, Y. Huang, A. M. Gorbach, and J. A. Rogers, Nat. Mater. **12**, 938 (2013).
[174]T. Dinh, H.-P. Phan, A. Qamar, P. Woodfield, N.-T. Nguyen, and D. V. Dao, J. Microelectromech. Syst. **26**, 966 (2017).
[175]K. M. Willett, N. P. Gillett, P. D. Jones, and P. W. Thorne, Nature **449**, 710 (2007).
[176]E. M. Fischer and R. Knutti, Nat. Clim. Change **3**, 126 (2013).
[177]A. V. Arundel, E. M. Sterling, J. H. Biggin, and T. D. Sterling, Environ. Health Perspect. **65**, 351 (1986).
[178]H. Farahani, R. Wagiran, and M. N. Hamidon, Sensors **14**, 7881 (2014).
[179]M. A. Islam, J. H. Kim, T.-J. Ko, C. Noh, S. Nehate, M. G. Kaium, M. Ko, D. Fox, L. Zhai, and C.-H. Cho, Nanoscale **10**(37), 17525–17533 (2018).
[180]Y. N. Guo, Z. Y. Gao, X. X. Wang, L. Sun, X. Yan, S. Y. Yan, Y. Z. Long, and W. P. Han, RSC Adv. **8**, 1078 (2018).
[181]H. Guo, C. Lan, Z. Zhou, P. Sun, D. Wei, and C. Li, Nanoscale **9**, 6246 (2017).
[182]D. H. Ho, Q. Sun, S. Y. Kim, J. T. Han, D. H. Kim, and J. H. Cho, Adv. Mater. **28**, 2601 (2016).
[183]T. Q. Trung, L. T. Duy, S. Ramasundaram, and N. E. Lee, Nano Res. **10**, 2021 (2017).
[184]P. G. Su and C. F. Chang, J. Taiwan Inst. Chem. Eng. **87**, 36 (2018).
[185]S. Borini, R. White, D. Wei, M. Astley, S. Haque, E. Spigone, N. Harris, J. Kivioja, and T. Ryhanen, ACS Nano **7**, 11166 (2013).
[186]G. E. Hofmann, J. E. Smith, K. S. Johnson, U. Send, L. A. Levin, F. Micheli, A. Paytan, N. N. Price, B. Peterson, Y. Takeshita, P. G. Matson, E. D. Crook, K. J. Kroeker, M. C. Gambi, E. B. Rivest, C. A. Frieder, P. C. Yu, and T. R. Martz, PLos One **6**, e28983 (2011).
[187]J. H. Guo, X. J. Liu, Y. Zhang, J. L. Shen, W. X. Han, W. F. Zhang, P. Christie, K. W. Goulding, P. M. Vitousek, and F. S. Zhang, Science **327**, 1008 (2010).
[188]R. Rahimi, M. Ochoa, A. Tamayol, S. Khalili, A. Khademhosseini, and B. Ziaie, ACS Appl. Mater. Interfaces **9**, 9015 (2017).
[189]D. Wencel, T. Abel, and C. McDonagh, Anal. Chem. **86**, 15 (2014).
[190]G. Wang, S. Zhang, S. Dong, D. Lou, L. Ma, X. Pei, H. Xu, F. Umar, W. Guo, and J. Luo, IEEE Trans. Biomed. Eng. (published online); https://ieeexplore.ieee.org/document/8440715.
[191]H. J. Chung, M. S. Sulkin, J. S. Kim, C. Goudeseune, H. Y. Chao, J. W. Song, S. Y. Yang, Y. Y. Hsu, R. Ghaffari, I. R. Efimov, and J. A. Rogers, Adv. Healthcare Mater. **3**, 59 (2014).
[192]S. Naficy, F. Oveissi, B. Patrick, A. Schindeler, and F. Dehghani, Adv. Mater. Technol. **3**, 1800137 (2018).
[193]W. Dang, L. Manjakkal, W. T. Navaraj, L. Lorenzelli, V. Vinciguerra, and R. Dahiya, Biosens. Bioelectron. **107**, 192 (2018).
[194]X. J. Liu, H. Q. Li, B. Y. Zhang, Y. J. Wang, X. Y. Ren, S. Guan, and G. H. Gao, RSC Adv. **6**, 4850 (2016).
[195]J. Lelieveld, J. S. Evans, M. Fnais, D. Giannadaki, and A. Pozzer, Nature **525**, 367 (2015).
[196]H. Akimoto, Science **302**, 1716 (2003).
[197]H. Yan, M. Zhong, Z. Lv, and P. Wan, Small **13**, 1701697 (2017).
[198]P. Gutruf, E. Zeller, S. Walia, H. Nili, S. Sriram, and M. Bhaskaran, Small **11**, 4532 (2015).
[199]Y. J. Yun, D. Y. Kim, W. G. Hong, D. H. Ha, Y. Jun, and H.-K. Lee, RSC Adv. **8**, 7615 (2018).
[200]Z. Song, Z. Huang, J. Liu, Z. Hu, J. Zhang, G. Zhang, F. Yi, S. Jiang, J. Lian, J. Yan, J. Zang, and H. Liu, ACS Sens. **3**, 1048 (2018).
[201]Y. Luan, S. Zhang, T. H. Nguyen, W. Yang, and J. S. Noha, Sens. Actuator B **265**, 609 (2018).
[202]Y. M. Fu, H. X. He, Y. Liu, Q. Wang, L. L. Xing, and X. Y. Xue, J. Mater. Chem. C **5**, 1231 (2017).
[203]K. H. Won, B. M. Weon, and J. H. Je, Curr. Appl. Phys. **17**, 339 (2017).
[204]H. B. Lee, C. W. Bae, L. T. Duy, I. Y. Sohn, D. I. Kim, Y. J. Song, Y. J. Kim, and N. E. Lee, Adv. Mater. **28**, 3069 (2016).
[205]E. Singh, M. Meyyappan, and H. S. Nalwa, ACS Appl. Mater. Interfaces **9**, 34544 (2017).
[206]Q. Hua, J. Sun, H. Liu, R. Bao, R. Yu, J. Zhai, C. Pan, and Z. L. Wang, Nat. Commun. **9**, 244 (2018).
[207]Z. Huang, Y. Hao, Y. Li, H. Hu, C. Wang, A. Nomoto, T. Pan, Y. Gu, Y. Chen, and T. Zhang, Nat. Electron. **1**, 473 (2018).
[208]P. H. Hoet, A. Nemmar, and B. Nemery, Nat. Biotechnol. **22**, 19 (2004).
[209]G. Oberdörster, A. Maynard, K. Donaldson, V. Castranova, J. Fitzpatrick, K. Ausman, J. Carter, B. Karn, W. Kreyling, and D. Lai, Part. Fibre Toxicol. **2**, 8 (2005).
[210]V. L. Colvin, Nat. Biotechnol. **21**, 1166 (2003).